



The α C helix of TIRAP holds therapeutic potential in TLR-mediated autoimmune diseases



Masaud Shah^{a,1}, Gi-Young Kim^{a,1}, Asma Achek^{a,1}, Eun-Young Cho^a, Wook-Young Baek^b, Yang Seon Choi^a, Wang Hee Lee^a, Dong-Jin Kim^c, Sang Ho Lee^c, Wook Kim^a, Soon Sun Kim^d, Jae Youn Cheong^d, Chang-Hee Suh^b, Sangdun Choi^{a,*}

^a Department of Molecular Science and Technology, Ajou University, Suwon, 16499, South Korea

^b Department of Rheumatology, Ajou University School of Medicine, Suwon, 16499, South Korea

^c Division of Nephrology, Department of Internal Medicine, Kyung Hee University Hospital at Gangdong, Seoul, 05278, South Korea

^d Department of Gastroenterology, Ajou University School of Medicine, Suwon, 16499, South Korea

ARTICLE INFO

Keywords:

Autoimmune disease
Toll-like receptor
Systemic lupus erythematosus
Psoriasis
Nonalcoholic steatohepatitis
Sepsis

ABSTRACT

Despite being crucial for combating microbes, paradoxical Toll-like receptors (TLRs) signaling have been associated with the aggravation of multiple immune disorders such as systemic lupus erythematosus, psoriasis, rheumatoid arthritis, and nonalcoholic steatohepatitis. The stoichiometry and precise arrangement of the interaction of adapters (via their Toll/interleukin-1 receptor [TIR] domains) are indispensable for the activation of TLRs and of downstream signaling cascades. Among adapters, plasma membrane-anchored MyD88 adaptor-like (MAL) has the potential for BB-loop-mediated self-oligomerization and interacts with other TIR domain-containing adaptors through α C and α D helices. Here, we used information on the MAL- α C interface to exploit its pharmacophores and to design a decoy peptide (MIP2) with broad-range TLR-inhibitory abilities. MIP2 abrogated MyD88- and TRIF-dependent lipopolysaccharide (LPS)-induced TLR4 signaling in murine and human cell lines and manifested a therapeutic potential in models of psoriasis, systemic lupus erythematosus, nonalcoholic steatohepatitis, and sepsis. Levels of hallmark serological and histological biomarkers were significantly restored and the disease symptoms were substantially ameliorated by MIP2 treatment of the animals. Collectively, our biophysical, *in vitro*, and *in vivo* findings suggest that MIP2 has broad specificity for TLRs and may be effective in modulating autoimmune complications caused by microbial or environmental factors.

1. Introduction

The signaling of Toll-like receptors (TLR), a family of pattern-recognizing receptors, is necessary for pathogen recognition by the innate immunity. TLR recognizes unique features of substances released by the dying/damaged cells or presented by a pathogen during infection; these features are known as danger- and pathogen-associated molecular patterns [1]. Upon recognition of the danger- or pathogen-associated molecular patterns, the Toll/interleukin-1 receptor (TIR) domains of TLR self-associate, which is essential for signal transduction [2]. The latter event subsequently leads to the recruitment of other TIR-containing adaptor molecules—including the TIR domain-containing adapter-inducing interferon β (TRIF/Toll-like receptor adaptor molecule 1 [TICAM-1]), the TIR domain-containing adaptor protein (TIRAP), myeloid differentiation primary response 88 (MyD88), and the

TRIF-related adaptor molecule (TRAM/TICAM-2)—and the activation of nuclear factor kappa-light-chain-enhancer of activated B cells (NF- κ B), interferon-regulatory factors (IRFs), and other transcription factors [3]. The recruitment mechanisms of adaptor proteins are not analogous for all TLRs. TLRs that transmit their signals through MyD88 can be MAL-dependent or can bind directly to the TLR TIR domain to induce the downstream signaling cascade. In contrast, TLR3 signaling is mediated by TRIF, independently of MyD88 and TRAM [4].

Knowledge about the precise arrangement of TLR TIR and adapter molecules is crucial for understanding the mechanisms by which the TLRs convey their signals. Many empirical [5,6] and *in silico* models [7] have been proposed to decipher the TIR-TIR molecular interactions. Nonetheless, owing to its complexity, the entire signalosome architecture remains to be delineated. Molecular docking analyses, mutagenesis, and x-ray crystallography analyses have been performed to

* Corresponding author.

E-mail address: sangdunchoi@ajou.ac.kr (S. Choi).

¹ These authors contributed equally to this work.

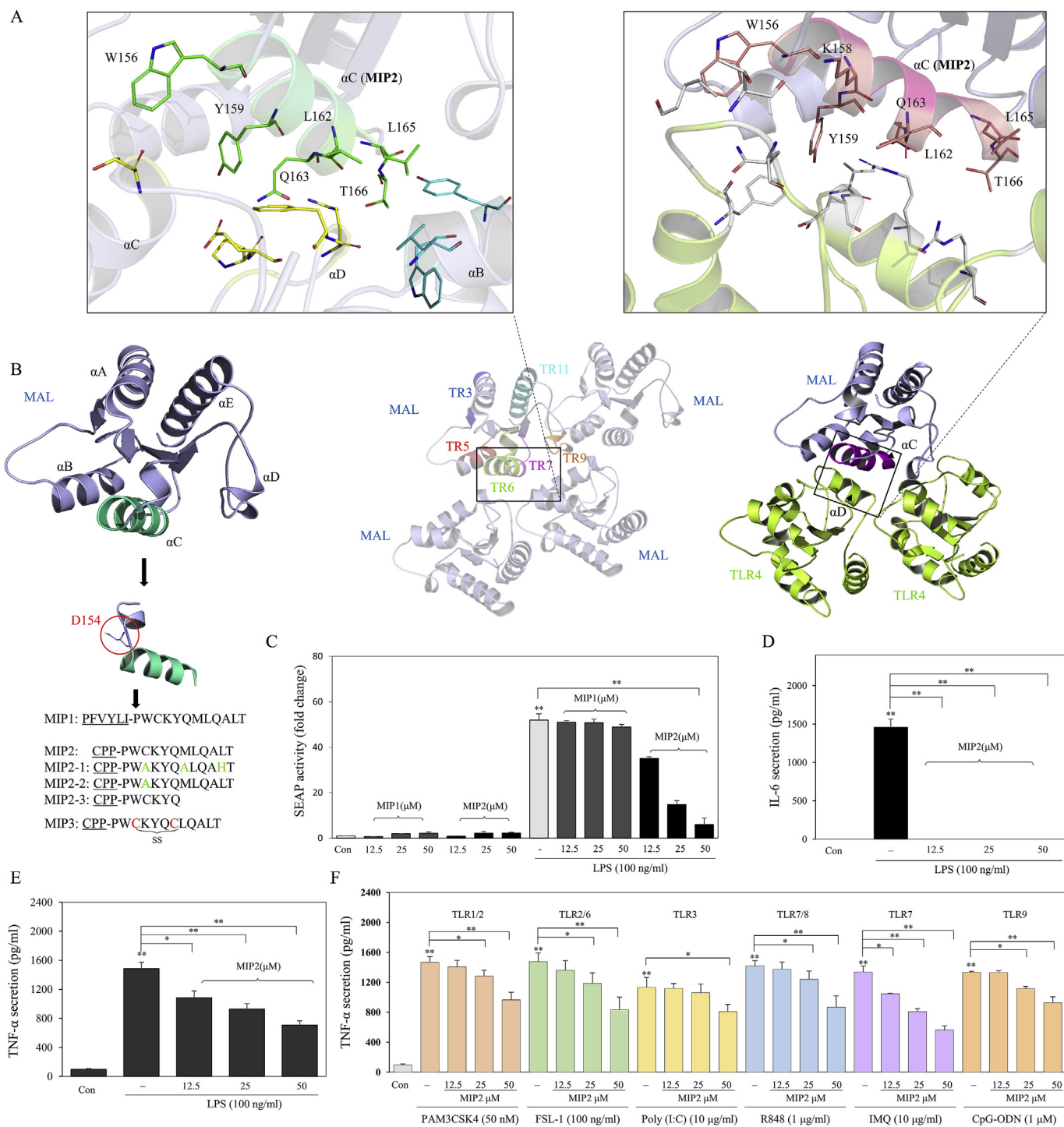


Fig. 1. Design of the peptides and *in vitro* screening. (A) The tetrameric complex of the MAL-TIR domains according to the cryo-EM structure of the MAL-TIR domain filament (Protein Data Bank ID: 5UZB) and the proposed MAL-TIR (Toll/interleukin-1 receptor) domain interaction with a modeled TLR4-TIR homodimer. The αC helix in MAL (labeled residues in the magnified insets) facilitates the TIR-TIR interaction. (B) The αC helix of MAL was chosen to design a MAL/MyD88-inhibitory peptide (MIP) and its derivatives. Aspartic acid (D154) has been depicted at the far end of the αC helix. (C) The TLR-inhibitory effects of MIP1 and MIP2 were evaluated on the HEK-Blue™ hTLR4 cells by measurement of the SEAP signals. (D, E) The secretion of IL-6 and TNF-α by the RAW 264.7 cells was evaluated through ELISA. (F) The broad-range TLR-inhibitory effect of MIP2 was evaluated by measurement of the TNF-α level in the RAW 264.7 cells; the cells were activated with PAM₃CSK₄ (acts on TLR2/1), FSL-1 (TLR2/6), poly(I:C) (TLR3), R848 (TLR7/8), imiquimod (IMQ, TLR7), or a CpG oligodeoxynucleotide (CpG-ODN; acts on TLR9) at various concentrations. The data represent at least three independent experiments ($n \geq 3$), and error bars indicate means \pm SD (* $P < 0.05$, ** $P < 0.01$). (For interpretation of the references to color in this figure legend, the reader is referred to the Web version of this article.)

propose the stoichiometric oligomerization of TIR-TIR models and unveil their interaction interfaces; still, for mammalian TIR domains, no common stoichiometric TIR-TIR interface has been identified [8]. Overall, the stoichiometric nature of the TIR-TIR interaction in the

signalosome has been hypothesized, and the mechanism underlying this interaction cascade is poorly understood.

Among the TIR domain-containing adapter proteins, MyD88 adaptor-like (MAL: TIRAP) has the capacity for bridging MyD88 with

TLR2 or TLR4 [9]. Lin et al. have reported that MAL-TIR can exist in a back-to-back symmetric dimer form, facilitated by the α C and α D helices and by the CD loop [9]. Conversely, cryoelectron microscopy (cryo-EM) has recently revealed that MAL TIR spontaneously and reversibly forms filaments *in vitro*, and this process is facilitated by the BB-loop [8]. According to the cryo-EM structure, MAL engages in intrastrand interactions (mediated by the BB-loop in a head-to-tail fashion) and in interstrand interactions (involving the α B and α C helices of one MAL TIR as well as the α D helix and CD loop of another MAL TIR; Fig. 1A). Thus, interstrand interactions are maintained in a triangular manner: i.e., one subunit interacts with two other subunits in a protofilament. This triangular interstrand interaction involving the α C helix is analogous to the dimeric symmetric interface suggested by Lin et al. [9].

Disruption of interstrand interactions via mutation of the residues W156, K158, Y159, L162, and L165 in the α C helix abrogates the MAL TIR filament formation [9]. The W156A mutation in α C substantially affects the MAL–MyD88 interaction [10,11]. Mutations at the symmetric interface can also disrupt the MAL–TLR4ic interactions in the mammalian protein–protein interaction trap experiments. Besides, a plausible interstrand interface, in a manner similar to the analysis of the MAL–MAL interstrand interface, has been suggested for the TLR4–TLR4–MAL TIR interaction (Fig. 1A) [8]. Altogether, these findings indicate the pivotal role of MAL– α C in TIR–TIR interactions and in stimulation of the downstream signaling cascade.

Considering the key function of MAL in TLR2 and TLR4 signaling, Couture et al. have designed the MAL-derived decoy peptides and reported their TLR4- and TLR2-antagonistic abilities [12]. Nonetheless, they suggested that a peptide derived from the n-terminal half of α C along with the CC loop (TR6)—but not the c-terminal half along with the CD loop (TR7)—could block the TLR2/1 and TLR4 signaling. Conversely, Lin et al. have reported that mutations Q163A and L165A (located at the c-terminus) can reduce the NF- κ B induction by 60% and 20%, respectively [9]. Similar results have been reported by Bovijin et al. [10]. Structural studies by Thomas et al. further support the role of L165 in MAL protofilament assembly [8]. Thus, we hypothesized that the c-terminal end of α C was as important as its n-terminal half, and that owing to the stable helical structure, a dodecapeptide (MAL/MyD88-inhibitory peptide [MIP] from here onward) comprising amino acid positions 155–166 (from P155 to T166), will be sufficient to prevent the MAL TIR assembly as well as other types of MyD88-dependent TLR signaling.

2. Methods

2.1. Peptide synthesis, reagents, and optimization of cell lines

The peptides were synthesized by Biostem (Ansan, Korea) at a purity of 97.09% (MIP1), 97.17% (MIP2), 95.1% (MIP3), and over 95% for other MIP2 derivatives, as determined by a reversed-phase high-performance liquid chromatography (HPLC; Shimadzu Prominence). For all the peptides, a Shiseido Capcell Pak C18 column (4.6×50 mm) was used with a 10%–60% acetonitrile gradient in 0.1% trifluoroacetic acid in water, at a flow rate of 1 mL/min, with detection at 220 nm. The molecular masses of the peptides were determined by means of the Shimadzu LCMS-2020. Lipopolysaccharide (LPS; *Escherichia coli* 0111:B4) and adenosine triphosphate (ATP) were purchased from Sigma-Aldrich (St. Louis, MO, USA). PAM₃CSK₄, poly(I:C), imiquimod (IMQ; R837), R848, and CpG oligodeoxynucleotide (CpG-ODN) were purchased from Thermo Fisher Scientific, Inc. (Waltham, MA, USA), whereas FSL-1 was purchased from InvivoGen (San Diego, CA, USA).

The RAW 264.7 and the HEK-Blue™ hTLR4 cells (InvivoGen) were cultured in a high-glucose Dulbecco's modified Eagle's medium (DMEM) containing 1% of a penicillin/streptomycin solution, 10% of fetal bovine serum (FBS; Thermo Fisher Scientific, Inc.), and 0.2% of normocin (InvivoGen). THP-1 cells were cultured in the RPMI 1640 medium

supplemented with 1% of the penicillin/streptomycin solution and 10% of FBS. These cells were differentiated into macrophages using 80 nM phorbol 12-myristate 13-acetate (PMA; Sigma-Aldrich) for 24 h. All the cells were incubated in a humidified atmosphere containing 5% of CO₂ at 37 °C (Thermo Fisher Scientific, Inc.), and media were changed after 18 h of incubation.

2.2. Cell viability assay

The HEK-Blue™ hTLR4 cells were seeded at a density of 5×10^4 /well, whereas the RAW 264.7 and THP-1 cells were seeded at 2×10^5 /well. All the cells were grown overnight in 96-well plates (BD Biosciences, San Jose, CA, USA). Cell viability was measured in a colorimetric 1-(4,5-dimethylthiazol-2-yl)-3,5-diphenylformazan [MTT] assay (Sigma-Aldrich) and/or 3-(4,5-dimethylthiazol-2-yl)-5-(3-carboxymethoxyphenyl)-2-(4-sulfophenyl)-2H-tetrazolium [MTS] assay (Promega, Madison, WI, USA).

2.3. Secreted embryonic alkaline phosphatase (SEAP) activity assay

The HEK-Blue™ hTLR4 cells were seeded in 24-well plates (BD Biosciences) at a density of 2×10^5 /well and were grown overnight. The cells were pretreated with different concentrations of the peptides for 1 h in the presence and/or absence of LPS (100 ng/mL, for 24 h). Aliquots of culture supernatants (200 μ L) from the treated cells were transferred to microcentrifuge tubes and heated for 10 min at 65 °C on a heating block (FINEPCR Co., Seoul, Korea). The culture supernatants were later placed in new 96-well plates (BD Biosciences), and SEAP production was quantified with the HEK-Blue™ Detection Kit (InvivoGen). Absorbance was measured on a microplate reader spectrophotometer system (Molecular Devices Inc., Silicon Valley, CA, USA) at 620 nm.

2.4. Enzyme-linked immunosorbent (ELISA) assays

The THP-1-derived macrophages and the RAW 264.7 cells were seeded at a density of 2×10^5 /well in 96-well plates (BD Biosciences) and grown overnight. After 24 h of treatment, IL-6 secretion was assayed by the Mouse IL-6 ELISA MAX™ Deluxe (BioLegend, San Diego, CA, USA), and TNF- α production was evaluated by means of the Mouse TNF alpha ELISA Ready-SET-Go!® Kit (eBioscience, San Diego, CA, USA). After 24 h of MIP2 treatment of the THP-1 cells, the secretion levels of IL-6 and TNF- α were assayed using the Human IL-6 or TNF alpha ELISA MAX™ Deluxe Kit (BioLegend), respectively. Absorbance was then analyzed on the microplate spectrophotometry system (Molecular Devices) at the appropriate wavelengths.

2.5. Protein quantification and Western blot analyses

Total-protein extraction was performed using the M-PER Mammalian Protein Extraction Reagent (Thermo Fisher Scientific, Inc.). The concentration of proteins was measured with the Bicinchoninic Acid (BCA) Assay Kit (Sigma-Aldrich). Western blot analysis, including gel electrophoresis and transfer, was conducted in a Mini-PROTEAN Tetra Cell and the Mini Trans-Blot Electrophoretic Transfer Cell System (Bio-Rad Laboratories, Hercules, CA, USA). The resultant membranes were immunoblotted with specific primary antibodies (mentioned below) at 1:500–1:1000 dilution with gentle shaking at 4 °C overnight. Antibodies against phospho-(p)-p65, p-JNK, JNK, p-IRF3, p-IRF7, p-ERK, ERK, p-p38, p38, I κ -B α , IL-1 β , NLPR3, and p-IRAK4 were purchased from Cell Signaling Technology Inc. (Danvers, MA, USA); against ATF3, cyclooxygenase 2 (COX2), and β -actin from Santa Cruz Biotechnology Inc. (Dallas, TX, USA); against nitric oxide synthase (iNOS) from BD Biosciences; and against p-c-Jun from Abcam (Cambridge, MA, USA). After that, the membranes were rigorously washed with phosphate-buffered saline (PBS) supplemented with 0.1%

of Tween 20 (PBST) and incubated with a peroxidase-conjugated anti-mouse or anti-rabbit IgG antibody (1:1000) for 2 h. The proteins were detected by means of a SuperSignal West Pico ECL solution (Thermo Fisher Scientific, Inc.) and visualized on a ChemiDoc™ Touch Imaging System (Bio-Rad Laboratories).

2.6. Quantitation of intracellular nitric oxide (NO) and reactive oxygen species (ROS) and extracellular NO production assay

The RAW 264.7 cells were seeded at a density of 10^6 cells per 6 cm culture dish (SPL Life Sciences, Pochun, Korea) and were grown overnight. After LPS stimulation and MIP2 treatment, intracellular NO and ROS levels were quantified by means of dyes, DAF-FM (4-amino-5-methylamino-2',7'-difluorofluorescein) and DCF-DA (2',7'-dichlorofluorescin diacetate; Thermo Fisher Scientific, Inc.) as per a previously described method [13]. Fluorescence intensity of the cells was analyzed on a FACS Aria III instrument with the Diva software (BD Biosciences). For assessment of the production of extracellular NO, the RAW 264.7 cells were seeded at a density of 2×10^5 /well and grown overnight in 96-well plates (BD Biosciences). Extracellular production of NO was measured with the Nitric Oxide Detection Kit (iNtRON Biotechnology Inc., Seongnam, Korea) as per a method described previously [13]. The absorbance was read on a microplate spectrophotometry system (Molecular Devices) at 550 nm.

2.7. Confocal microscopy

The RAW 264.7 and the NIH3T3 cells were seeded at a density of 2×10^5 and 5×10^4 /well, respectively, in 24-well plates (BD Biosciences). The RAW 264.7 cells were treated with MIP2 (50 μ M) for 1 h before LPS stimulation (100 ng/mL) for 30 min. The NIH3T3 cells were pretreated with the fluorescein isothiocyanate-conjugated MIP2 (FITC-MIP2; 20 μ M) for 1 h and were activated with LPS (100 ng/mL) for 30 min. All cells were fixed in a 3.7% formaldehyde solution (Sigma-Aldrich) and permeabilized with a 0.2% Triton X-100 solution (AMRESCO, Solon, OH, USA) for 15 min. The cells were then washed with PBS and blocked with a 2% BSA solution (Thermo Fisher Scientific, Inc.). The RAW 264.7 cells were incubated with the anti-p65 (1:1000; Cell Signaling Technology Inc.) and anti-p-p65 antibodies (1:1000; Santa Cruz Biotechnology Inc.), while the NIH3T3 cells were incubated with the anti-TIRAP (1:500; Abcam) and anti-MyD88 antibodies (1:500; Santa Cruz Biotechnology Inc.) for 2 h and rigorously washed with PBS. Next, the cells were incubated with an Alexa Fluor 546-conjugated (Invitrogen, Carlsbad, CA, USA) or an Alexa Fluor 594-conjugated (Abcam) secondary antibody for 1 h and washed with PBS three times. A Hoechst 33258 solution (5 μ M; Sigma-Aldrich) was employed to stain the nuclei. Fluorescence intensities were measured by confocal microscopy (LSM-700; Carl Zeiss Microscopy GmbH, Munich, Germany), and images were analyzed with the Zen 2009 software.

2.8. Surface plasmon resonance (SPR) spectroscopy

The SPR analyses were conducted on the Biacore T200 (GE Healthcare, Sweden) to assess the biophysical interaction of MIP2 with the TIR domain-containing proteins (TLR4-TIR, MyD88-TIR, and TIRAP). MIP2 was immobilized onto the surface of the CM5 sensor chip (GE Healthcare) at a concentration of 1.85 μ g/mL using a 10 mM sodium acetate solution (pH 6.0). PBST (0.005% of Tween 20) was used as the running buffer and a 10 mM glycine (pH 1.5) solution as a regeneration buffer. The TIR domains of TLR4, MyD88, and TIRAP were synthesized by Bioneer (Daejeon, Korea) and injected into the MIP2-bound chip at various concentrations ranging from 0 μ M to 2 μ M. The running buffer was injected into the empty channel as a reference. The experiments were conducted in duplicate with freshly prepared reagents, and the data were analyzed in the Scrubber2 software.

2.9. The procedure for animal experiments

2.9.1. A mouse model of psoriasis

C57BL/6J mice aged 6–7 weeks were purchased from Orient Bio Inc. (Seongnam, South Korea) and housed under specific pathogen-free conditions with a standard laboratory diet *ad libitum*. The psoriasis-related animal experiments were approved by the Institutional Animal Care and Use Committee (IACUC) at the Ajou University (Approval No. 2017-0002). Psoriasis-like symptoms were generated by topical application of 62.5 mg of Aldara cream (containing 5% of IMQ; Aldara, 3M Pharmaceutical LLC), for 5 consecutive days. IMQ was not applied to the normal group, which was intraperitoneally (i.p.) injected with PBS only. Mice received daily doses of MIP2 (1 nmol/g, 10 nmol/g, or 20 nmol/g) or PBS as a control, 1 day before the application of Aldara cream (5%). Methotrexate (MTX; 10 μ g/g; cat. #M9929, Sigma-Aldrich) was administered as the positive control 1 day before application of the IMQ cream. After 5 days, the mice were euthanized under respiratory anesthesia, and skin lesions and spleen samples were collected for a histological examination. To score the inflammation severity of the back skin, an objective scoring system was developed based on the Psoriasis Area and Severity Index (PASI, a tool widely used for the assessment of psoriasis severity in the clinic). Factors like erythema, scaling, wrinkles, and thickening were scored independently on the scale from 0 to 4 as follows: 0, none; 1, slight; 2, moderate; 3, substantial; and 4, very well pronounced. Erythema, scaling, and thickness were scored under careful supervision of experienced researchers. The cumulative score (erythema plus scaling plus thickening scores, scale 0–12) indicated the severity of the psoriasis symptoms.

Skin samples from the back lesions were fixed in a 4% paraformaldehyde solution, embedded in paraffin, sectioned at 7- μ m thickness, and placed onto glass slides. The sections were stained with hematoxylin and eosin (H&E) to evaluate the thickness of the epidermis and dermis. The thickness of the skin was measured under a Leica DMi8 fluorescence microscope using a Leica LAS X Hardware Configurator. IMQ-induced inflammation in the skin was evaluated by means of the mouse-specific HRC/DAB Detection IHC Kit (Abcam, cat. # AB64259) with primary antibodies recognizing CD68, CD4, and IL-17.

2.9.2. A mouse model of systemic lupus erythematosus (SLE)

Six female wild-type (C57BL/6) and six lupus-prone mice (MRL/lpr), initially weighing 18 g–20 g and 38 g–40 g, respectively, were purchased from the Jackson Laboratory (Bar Harbor, ME, USA). Similar to the psoriasis model, the SLE-related animal procedures were reviewed and approved by the IACUC at the Ajou University Medical Center (Approval No. 2017-0022). The mice were allowed to acclimate for 1 week and were bred under specific pathogen-free conditions according to the approved guidelines. The mice in the vehicle group were i.p. injected with PBS, while others with MIP2 at a dose of 10 nmol/g per day (in PBS) for 20 days (5 times/week for 4 weeks), and their weight was monitored on a daily basis. The mice were euthanized at the end of the experiments, and their blood, urine, and relevant tissues were collected. After 1 h incubation, blood samples were collected into serum separation tubes, centrifuged at 3000 rpm for 10 min at 20 °C and stored at –80 °C. The collected urine samples were immediately stored at –80 °C, whereas the tissue samples were thoroughly washed with PBS and immersed in the RNA Stabilization Solution (Qiagen Sciences, Maryland, MD, USA). The concentrations of antinuclear antibodies (ANA), anti-dsDNA antibodies, IL-6, and C3 complement component were analyzed with ELISA kits (MyBiosource, San Diego, CA). The urinary albumin levels were determined with the Mouse Albumin ELISA Kit (41-ALBMS-E01, Alpco Diagnostics, Salem, NH, USA). The kidney tissues were collected and then fixed in 4% paraformaldehyde and refrigerated overnight at 4 °C. Next, the fixed tissues were paraffin-embedded, sectioned at 2- μ m to 4- μ m thickness, and stained with the periodic acid-Schiff (PAS) or H&E reagents. Three independent measurements were performed per sample.

2.9.3. A mouse model of nonalcoholic steatohepatitis (NASH)

Twenty-four male wild-type (C57BL/6J) mice, aged 9 weeks, initially weighing 21 g–28 g, were purchased from Japan SLC, Inc. (Shizuoka, Japan). From the age of 10 weeks, the mice were separated into four groups of six animals. The control group was fed with a normal chow diet, the methionine-and-choline-deficient (MCD) diet group was fed with the MCD diet, the MIP2 prevention group was fed with the MCD diet and treated with MIP2 from the beginning, and the MIP2 treatment group was fed with the MCD diet and MIP2 was administered starting from the third week. The mice in the control and the MCD groups were i.p. injected with PBS, while others were injected with MIP2 at a dose of 10 nmol/g per day (in PBS) for 6 weeks (7 times/week). Their weight was monitored on a daily basis. The mice were euthanized at the end of the experiments, and their blood and liver tissue samples were collected. After 1 h incubation, blood samples were collected into serum separation tubes, centrifuged at 3000 rpm for 10 min at 20 °C, and stored at –80 °C. A liver lysate was prepared with the RIPA buffer (Biosesang, R2002, Korea). Triglycerides in the liver lysate were quantitated using the Triglyceride Quantification Colorimetric Kit (Biovision K622-100, Inc.). Cholesterol in the liver lysate was measured with the Total Cholesterol and Cholestryl Ester Colorimetric Kit (Biovision K603-100, Inc.). Quantitative reverse-transcription PCR (qRT-PCR) analysis was performed on an ABI Prism 7500 qRT-PCR system (Applied Biosystems, Foster City, CA, USA). Gene expression was measured with the SYBR Premix Ex Taq (Takara RR420A, Inc.), and the relative gene expression was determined by normalization to a reference gene, GAPDH, with the delta-delta C_t method ($2^{-\Delta\Delta C_t}$). All the experiments were performed at least three times, and each result has been reported as mean ± SD. One-way ANOVA with a *post hoc* test was conducted for all statistics (in figures, the results have been labeled as *P < 0.05; **P < 0.001; ***P < 0.0001 compared to the MCD group). The NASH-related animal procedures were reviewed and approved by the IACUC at Biotoxtech Co., Ltd. (Cheongju, South Korea) (Approval No. 180798).

2.9.4. The therapeutic benefit of MIP2 in the mouse model of LPS-induced sepsis

Eight-week-old C57BL/6 mice (20 g–25 g, n = 12) were purchased from Dae Han Bio Link Co., Ltd. (Seoul, Korea). Mice were i.p. injected with MIP2 (10 nmol/g) 1 h before the LPS injection (5 µg/g). The control group was injected with PBS. At 2 h and 24 h after the LPS injection, the plasma samples were collected and stored at –80 °C until analysis was performed for IL-1β, TNF-α, IL-6, and the vascular endothelial growth factor (VEGF). Plasma levels of IL-1β, TNF-α, IL-6, and VEGF was evaluated using the Magnetic Luminex Screening Assay, Mouse Premixed Multi-Analyte Kit (R&D Systems Inc., Minneapolis, MN, USA). The levels of blood urea nitrogen (BUN) and creatinine (Cr) in the plasma samples were measured with a VETTEST-8008 system (IDEXX, Ludwigsburg, Germany). Kidney tissue slices were obtained by cutting along the sagittal plane, and the obtained tissues were fixed in a 10% formalin solution overnight, embedded in paraffin wax, and cut into 4 µm thick slices on a microtome. Apoptotic cells were then quantified by staining them with a terminal deoxynucleotidyl transferase dUTP nick end labeling (TUNEL) Staining Kit (Merck Millipore, Billerica, MA, USA) and were visualized by confocal microscopy (the LSM-700 microscope, Carl Zeiss GmbH, Munich, Germany) using the Zen 2009 software package.

2.9.5. The survival rate under the influence of LPS in the *in vivo* model of sepsis

Eight-week-old BALB/c mice (20 g–25 g, n = 10 or 12) were injected i.p. with MIP2 (10 nmol/g) 1 h before the injection of LPS (5 µg/g or 10 µg/g). The control group was injected with PBS. The day of injection was referred to as day 0, and the survival rates were recorded for up to 3 days post injection. All the animal experiments were approved by the Institutional Animal Care and Use Committee (approval

number: KHNMC AP 2019–014).

2.10. Statistical analysis

All data analyses were performed by the *t*-test in the SigmaPlot software (version 12.0, Systat Software Inc., San Jose, CA, USA) or the GraphPad Prism 5 (GraphPad Software, Inc., San Diego, CA, USA). All experiments were conducted independently at least three times, and statistical significance was defined as a *P*-value of *P < 0.05, **P < 0.01.

3. Results

3.1. Peptide design and *in silico* analyses

In-depth analysis of the MAL symmetric or interstrand interface has highlighted the pivotal role of αC in MAL-MAL, MAL-TLR4, and MAL-MyD88 TIR-TIR interactions (Fig. 1A). In an NF-κB reporter assay, Lin et al. found that MAL mutations W156A, Y159A, and L165A, but not D154A, significantly affected the NF-κB signals [9]. Valkov et al. in their MAL structural studies have also found through alanine scanning that residues 162–166 in MAL are not only involved in MAL self-association but are also crucial for the MAL-MyD88 association [11]. Collectively, these findings suggest that residues from P155 to T166 in MAL αC are important for the TIR-TIR interaction. Thus, the αC-binding interfaces in MAL, TLR, and MyD88 share some common pharmacophores that may be engaged by αC itself or by its mimics.

A dodecapeptide was designed from the αC helix and was vetted for structural stability and for the cell membrane penetration ability. To facilitate the entry of the MIP into the cell, the peptide was conjugated with a known cell membrane-penetrating peptide (CPP) with sequence PFVYLI (referred to as PFV below [14], and the fusion peptide was designated as MIP1) or penetratin [15] [RQIKIWFQNRRMKWKK, labeled as MIP2]. To maintain the helicity and structural stability of MIP2, after it was initially found to be safe (Supplementary Fig. 1A) and effective in the initial *in vitro* evaluation (Fig. 1B), a structural constraint was applied by creating a disulfide bond between C157 and C161 (thus resulting in MIP3; methionine at position 7 in the parent peptide was mutated to cysteine; Fig. 1B). Nevertheless, MIP3 exerted a cytotoxic effect at the tested concentrations (Supplementary Fig. 1A) and was not chosen for a further evaluation. The involvement of the c-terminal residues, especially L165, in the TLR-inhibitory effect was confirmed by the creation and testing of MIP2 variants. MIP2-1 (a triple mutant containing substitutions C157A, M161A, and L165H) lacks the ability to inhibit the LPS-stimulated TLR4 signaling. This loss of the effect was relatively small in case of MIP2-2 (a single mutant: C157A), which retained its inhibitory property (Supplementary Fig. 1B). MIP2-3, lacking residues MLQALT at its c-terminus, was completely devoid of the ability to inhibit the LPS-induced NO and TNF-α secretion by the RAW 264.7 cells.

MIP1 and MIP2 were further assessed for their modulatory effects on a MAL-mediated pathway. MIP2, but not MIP1, caused a dose-dependent inhibition of the LPS-stimulated SEAP signals in the HEK-Blue™ hTLR4 cells (Fig. 1A). This result suggested that 1) either hydrophobic PFVYLI has a poor cell membrane-penetrating ability when conjugated with the MIP or 2) penetratin has an additional TLR4-inhibitory effect when bound to the MIP. Besides, in our ongoing study (data not shown), we observed that a PFV-conjugated peptide bound to an extracellular target. To exclude the possibility that the CPPs may have a modulatory influence on the MIP, the two CPPs were individually tested, but there was no effect on the TNF-α secretion by the LPS-stimulated RAW 264.7 cells (Supplementary Fig. 1C). The unconjugated MIP was also tested, however, no effect was noted either. Similar results have been reported previously where a pep5–CPP conjugate, but not CPP or pep5 individually, was effective at inducing cell death [16]. The inhibitory action of MIP2 was then evaluated in comparison with our

previously reported CPP-conjugated peptide, TIP2 [17], which was inactive in terms of modulation of the TLR signaling (Supplementary Fig. 1C). These observations confirmed that MIP2 retained the TLR4-inhibitory property of MIP, and that penetratin was an effective carrier peptide (CPP) in this case.

3.2. MIP2 is a broad-range TLR inhibitor and abrogates MyD88- and TRIF-dependent TLR4 signaling in mouse macrophages

To determine whether MIP2 had a broad-range TLR-inhibitory effect and halted the MyD88- and TRIF-dependent TLR4 signals, we performed additional experiments on the RAW 264.7 cells. In the absence of any cytotoxic action at a concentration of 50 μ M and lower concentrations (Supplementary Fig. 1A), MIP2 abrogated the IL-6 secretion and significantly reduced the TNF- α secretion by the LPS-stimulated cells (Fig. 1D and E). To assess the effects of MIP2 on other TLRs, TNF- α and IL-6 secretion levels of the RAW 264.7 cells were measured after stimulation with different TLR ligands: PAM₃CSK₄ (TLR1/2), FSL-1 (TLR2/6), poly(I:C) (TLR3), resiquimod (R848; TLR7/8), imiquimod (IMQ; TLR7), or CpG oligodeoxynucleotide (ODN; TLR9). All TLRs, except TLR3, were found to be inhibited in a dose-dependent manner, whereas this effect was relatively more pronounced for TLR7 as compared to other TLRs (Fig. 1F and Supplementary Fig. 1D). The effect was almost the same for TLR2/1 and TLR2/6. Conversely, Couture et al. have observed that TR6 significantly inhibits the P3C (TLR2/1 ligand)-induced upregulation of mRNA levels of TNF- α and IL-1 β but not that of the P2C (TLR2/6 ligand)-induced effect [12]. Overall, these data confirmed that MIP2 significantly inhibited the extracellular as well as the endosomal TLRs; these findings point to a broad-range TIR domain-inhibitory potential of MIP2.

Consistent with these data, our Western blot results suggested that MIP2 substantially inhibited the phosphorylation of ERK, JNK, p38, and c-Jun (Fig. 2A). Conversely, TR6 has been reported to inhibit ERK, but not JNK, in the LPS-stimulated primary peritoneal macrophages [12]. There is an evidence that shows that TLR4 activates interferons only through the TRAM-TRIF pathway, whereas NF- κ B can be activated through both MyD88 and TRIF [18]. It has been confirmed that MAL and TRAM bind subsequently and facilitate the interaction of TRIF or MyD88 with TLR4 [19]. Consequently, we propose that MIP2 may be able to block both the pathways of TLR4. Of note, MIP2 abrogated the phosphorylation of IRF3 and expression of ATF3 in the LPS-stimulated RAW 264.7 cells (Fig. 2B). This phenomenon was replicated in the THP-1 cells, where MIP2 inhibited the phosphorylation of IRF3 and IRF7 (as discussed below). Nonetheless, we did not perform further assays to confirm the induction of type I IFN because IRF3 expression and IFN production are interdependent [20].

The TLR4-inhibitory property of MIP2 was next confirmed via an ectopic expression and analysis of the nuclear-translocation levels of NF- κ B. Western blot data confirmed that MIP2 attenuated the LPS-induced phosphorylation of NF- κ B (p-p65) and halted I κ -B α degradation (Fig. 2C). This result was confirmed by confocal microscopy, where MIP2 reduced the phosphorylation and nuclear translocation of the p65 subunit of NF- κ B (Fig. 2D). Stimulation of TLRs has been reported to be associated with the induction of NO and ROS production and the expression of related enzymes such as iNOS and COX2 [21,22]. MIP2 abrogated the expression of iNOS and COX2 (Fig. 2E), the extracellular and intracellular release of NO (Fig. 2F and G, respectively), and the production of intracellular ROS (Fig. 2H).

3.3. MIP2 inhibits TLR and NLRP3 pathways in THP-1 cells

In line with the findings in RAW 264.7 cells, MIP2 exerted inhibitory actions on MAPKs in LPS-stimulated THP-1-derived macrophages. Although p38 expression was inhibited only slightly in MIP2-treated RAW 264.7 cells, we observed that this phenomenon was more prominent in LPS-stimulated THP-1 cells (Fig. 3A). The amounts of p-

p65 and other transcription factors, p-ERK and p-JNK, were substantially lower in LPS-stimulated cells. Corroborating these data, MIP2 dose-dependently attenuated the TNF- α and IL-6 secretion by the LPS-stimulated cells (Fig. 3B). Growing evidence has confirmed that TLRs up-regulate expressions of NLRP3, caspase 1, and pro-IL-1 β [23–25]. In the absence of a second signal such as ATP, nigericin, streptolysin O, or uric-acid crystals, the LPS-primed cells have been reported to up-regulate pro-IL-1 β , but have reportedly failed to be processed into mature IL-1 β and to be released [26]. Furthermore, TLRs use both MyD88 and TRIF pathways to prime and activate the NLRP3 inflammasome [27]. This notion is supported by our Western blot experiments, where the LPS-primed cells expressed NLRP3 upon ATP treatment. Nonetheless, the expression of both NLRP3 and pro-IL-1 β was substantially lower in the presence of MIP2 (Fig. 3C). The induction of mature IL-1 β was significantly inhibited by MIP2 in the LPS-primed ATP-treated cells (Fig. 3C, bottom). In addition to IRF3, IRF7 is also expressed downstream of TLR4 in a TRIF-dependent manner [28]. Consistently with the findings in the RAW 264.7 cells, MIP2 abrogated the expression of not only IRF3 but IRF7 as well. Besides, the expression of pro-IL-1 β and p-IRAK4 was abrogated by MIP2 in the LPS-stimulated cells (Fig. 3D). These findings suggested that MIP2 was not only capable of affecting MyD88- and TRIF-dependent cytokine production but also inhibited the TLR-mediated NLRP3 inflammasome.

3.4. MIP2 interaction with the TIR domain-containing proteins

To confirm the potential binding of MIP2 to the TIR domains of TLR4, MyD88, and TIRAP, we used confocal cell imaging and SPR techniques. Our confocal data showed that the cotreatment of NIH3T3 cells with LPS and FITC-MIP2 (Fig. 4A, green color) resulted in the colocalization of the peptide with TIRAP (red color) and produced a cherry coloration (Fig. 4A, merged images). Similarly, FITC-MIP2 turned out to be colocalized with MyD88 (Fig. 4B, yellow color) and resulted in a lime color (merged images). These data were further supported by a biophysical interaction of MIP2 with the TIR domains of TLR4, MyD88, and TRAP, as confirmed through SPR. All three TIR domains bound to the immobilized MIP2 in a dose-dependent manner, as shown in the SPR sensogram (Fig. 4C). The calculated association (k_a) and dissociation (k_d) rate constants were found to be $7.38 \times 10^3 \text{ M}^{-1} \text{ s}^{-1}$ and $25.6 \times 10^{-4} \text{ s}^{-1}$ for MIP2-MyD88, $4.88 \times 10^3 \text{ M}^{-1} \text{ s}^{-1}$ and $23.02 \times 10^{-4} \text{ s}^{-1}$ for MIP2-TIRAP, and $2.65 \times 10^3 \text{ M}^{-1} \text{ s}^{-1}$ and $15.8 \times 10^{-4} \text{ s}^{-1}$ for MIP2-TLR4, respectively. These results suggest that the inhibitory effect of MIP2 on multiple TLR signaling pathways is likely due to its potential binding to the TIR domain-containing proteins.

3.5. MIP2 ameliorates IMQ-induced psoriasis in mice

Psoriasis is a chronic inflammatory skin disease characterized by an amplified proliferation and an altered differentiation of the epidermal cells as well as the inflammatory-cell infiltration into the skin [29]. TLRs have been widely shown to be linked with the onset and progression of psoriasis [30,31]. To test whether MIP2 held promise for healing the TLR-induced psoriasis, we induced the disease in 6- to 7-week-old C57BL/6 mice by the topical application of 62.5 mg of 5% IMQ cream to their back skin for 5 consecutive days (Fig. 5A). MIP2 was i.p. injected for 6 days at doses of 1 nmol/g, 10 nmol/g, or 20 nmol/g of mouse weight. The same protocol (details have been provided in the Methods) was applied to the MTX- and the PBS-injected mice. Comparative phenotypic examination suggested that MIP2 alleviated the disease symptoms, similar to that observed in MTX (Fig. 5A). The symptoms remained progressive and prominent in the PBS-injected mice. The PASI data revealed that even though a dose-dependent influence was not observed, MIP2 treatment substantially reduced the PASI score (Fig. 5B). Splenomegaly has been widely associated with psoriasis [32,33]. A dose-dependent reduction in the spleen weight was

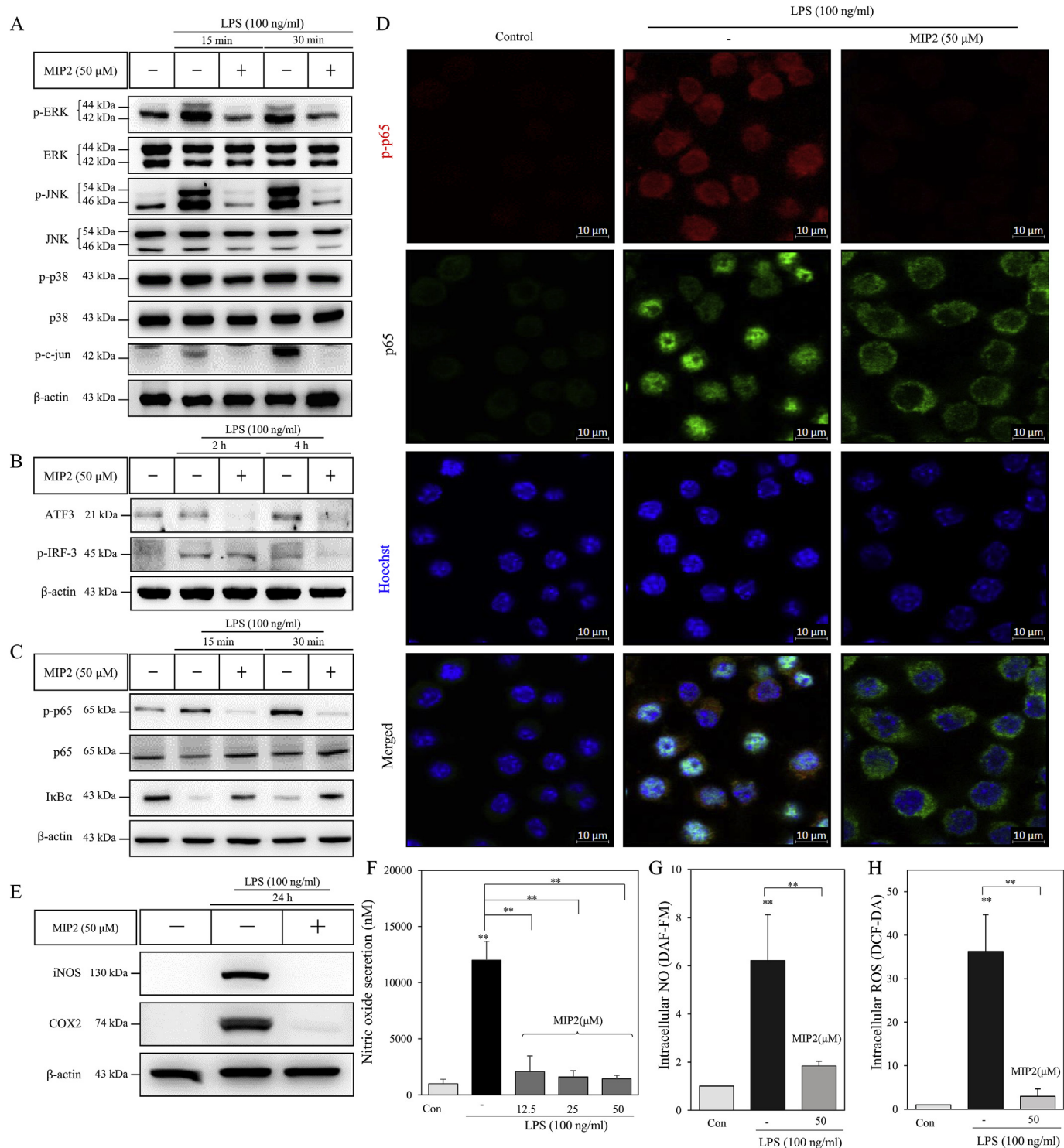


Fig. 2. MIP2 blocks the MyD88- and the TRIF-dependent TLR4 signaling in mouse macrophages. (A–C) The protein levels of phospho- (p)-p65, p65, I κ B α , p-c-Jun, ATF3, p-IRF3, p-ERK, ERK, p-JNK, JNK, p-p38, and p38 were measured by Western blot analysis of the total-protein extracts from RAW 264.7 cells, where β -actin served as a loading control. (D) NF- κ B (p65, green color), and its phosphorylated subunit (p-p65, red color) were evaluated by immunofluorescent staining and confocal microscopy. A histogram of quantitative data on the fluorescence intensity of p-p65 has been shown in Supplementary Fig. 2E. Hoechst 33258 was utilized for nuclear staining (the scale bar represents 10 μ m). (E) The expression of iNOS and COX2 was completely inhibited by MIP2 as evidenced by western blotting; β -actin served as a loading control. (F) The NO secretion level was evaluated using a standard NO secretion kit. (G, H) Intracellular production of NO and reactive oxygen species (ROS) was quantified by DAF-FM (4-amino-5-methylamino-2',7'-difluorofluorescein) and DCF-DA (2',7'-dichlorofluorescin diacetate) staining, respectively, and these parameters were found to be substantially down-regulated by MIP2. Histograms of the quantitative data on all the analyzed proteins and their band intensities have been presented in Supplementary Fig. 2C. The data represent at least three independent experiments ($n \geq 3$), and error bars denote mean \pm SD (* $P < 0.05$, ** $P < 0.01$). (For interpretation of the references to color in this figure legend, the reader is referred to the Web version of this article.)

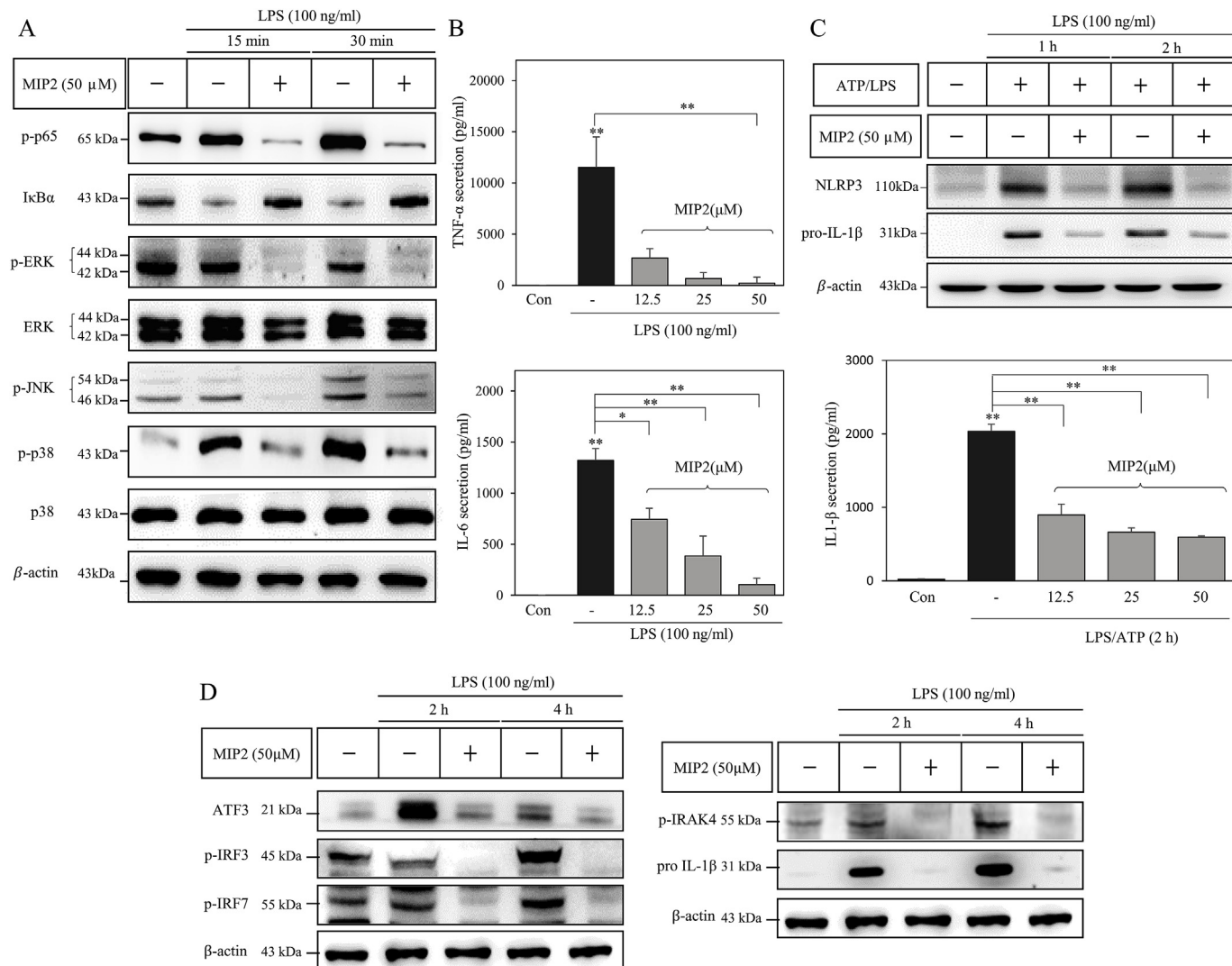


Fig. 3. MIP2 inhibits the TLR and the NLRP3 pathways in the THP-1 cells. (A) Multiple transcription factors including phospho- (p-)p65, IκBα, p-ERK, ERK, p-JNK, JNK, p-p38, and p38 were quantitated by western blotting, where β-actin served as a loading control. The phosphorylation of these factors was substantially inhibited by MIP2. (B) The secretion levels of TNF-α and IL-6 were evaluated through ELISA assays. (C) The inhibitory effects of MIP2 on NLRP3 were evaluated in the lipopolysaccharide (LPS)-primed (100 ng/mL for 4 h) ATP-treated (10 mM) THP-1 cells. The expression levels of NLRP3 and pro-IL-1β were measured by western blotting, and the secretion of cytokine IL-1β was assessed using an ELISA. (D) The amounts of ATF3, p-IRF3, p-IRF7, p-IRAK4, and pro IL-1β were evaluated in the LPS-stimulated cells by Western blot analysis, and β-actin served as a loading control. Histograms of quantitative data on all the tested proteins and their band intensities have been given in Supplementary Fig. 2D. The data represent at least three independent experiments ($n \geq 3$), and error bars denote mean \pm SD (* $P < 0.05$, ** $P < 0.01$).

noted in the MIP2-treated mice (Fig. 5C). Body weight-monitoring data did not reveal any significant difference from the PBS- and the MTX-treated mice (Fig. 5D). The histopathological changes in the skin were evaluated through H&E staining; thickness of the epidermis (Fig. 5E, yellow arrowheads) and the dermis (green arrowheads) were substantially lower in the MIP2-treated mice. The hyperproliferative state of the skin and immune-cell infiltration (T cells or macrophages) are considered the major hallmarks of psoriasis [31]. Hence, the skin lesions were collected from each mouse group and were analyzed by immunohistochemical techniques using anti-CD68 (macrophage marker) and anti-CD4 and anti-IL-17 (T helper 17 [Th17] cell markers) antibodies. MIP2 substantially attenuated the overexpression of CD68, CD4, and IL-17 (Fig. 5F, brown staining) in psoriatic mice. Despite significance of the results, the therapeutic effect of MIP2 was not consistent at 20 nmol/g. This dose was almost double of the highest concentration (50 μM) used in our *in vitro* experiments. Taking these observations into consideration, we conducted the subsequent animal experiments at 10 nmol/g. Collectively, these data suggest that MIP2

may hold promise for ameliorating the induced psoriatic symptoms. Considering that this phenomenon could be due to TLR7, which is a common target of IMQ (to induce psoriasis) and MIP2 (blocks TLR7 signaling), we next evaluated the therapeutic activities of MIP2 in the MR/lpr mice, as discussed below.

3.6. The therapeutic benefit of MIP2 in the mouse model of SLE

The severity and pathogenesis of SLE, a disease characterized by the lack of the body's tolerance to the self-nuclear antigens, have been widely associated with the up-regulation of TLR. This observation has been confirmed in experimental animal models, clinical studies, and genome-wide association studies [34]. Hence, we decided to evaluate the therapeutic potential of MIP2 in a murine model of SLE. MRL lymphoproliferation mice (a.k.a. MRL/lpr mice: these animals spontaneously present with hallmark serological signs and peripheral pathologies typifying lupus) were i.p. injected with MIP2 for 20 days, at a daily dose of 10 nmol/g of the mouse weight (the protocol has been

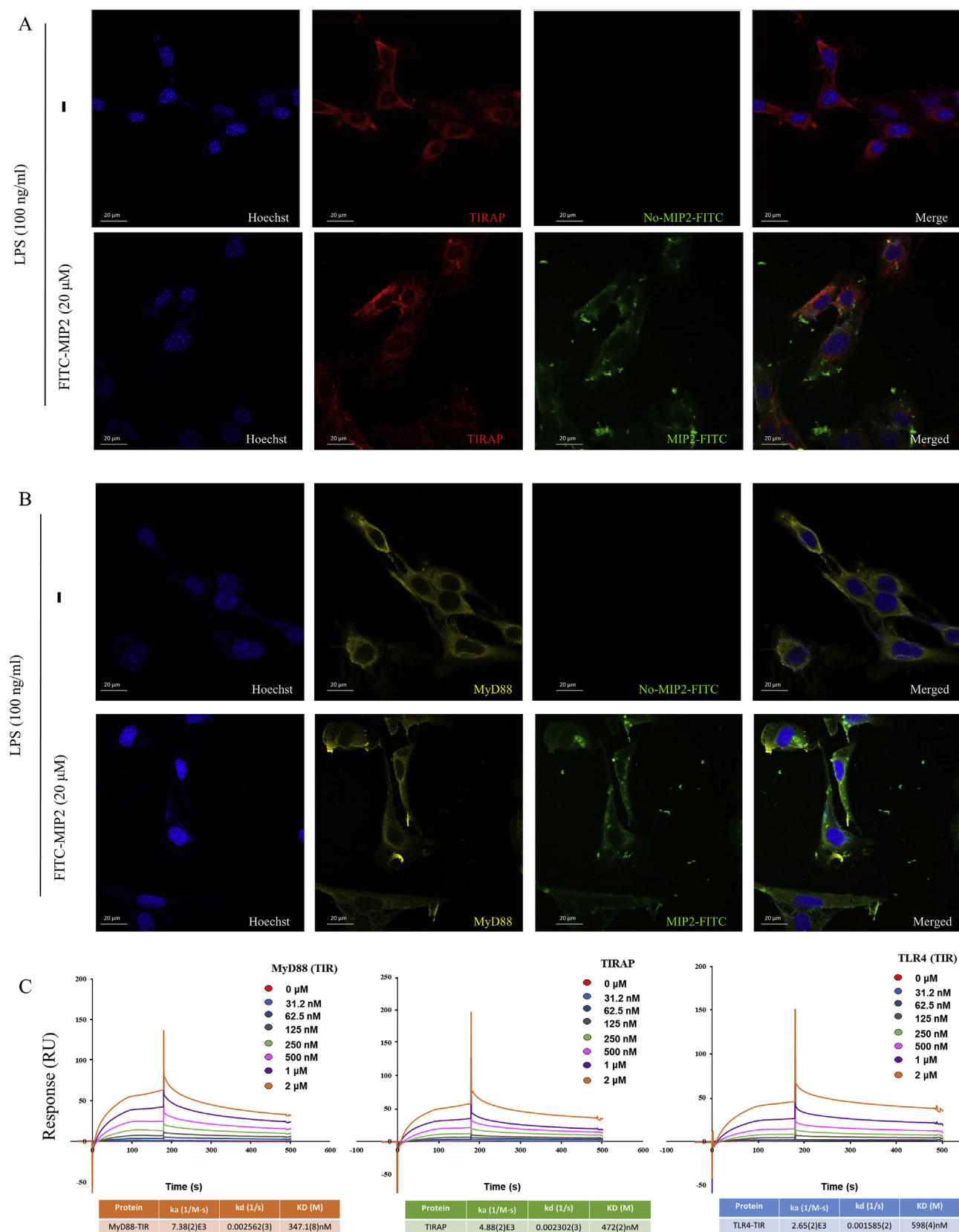
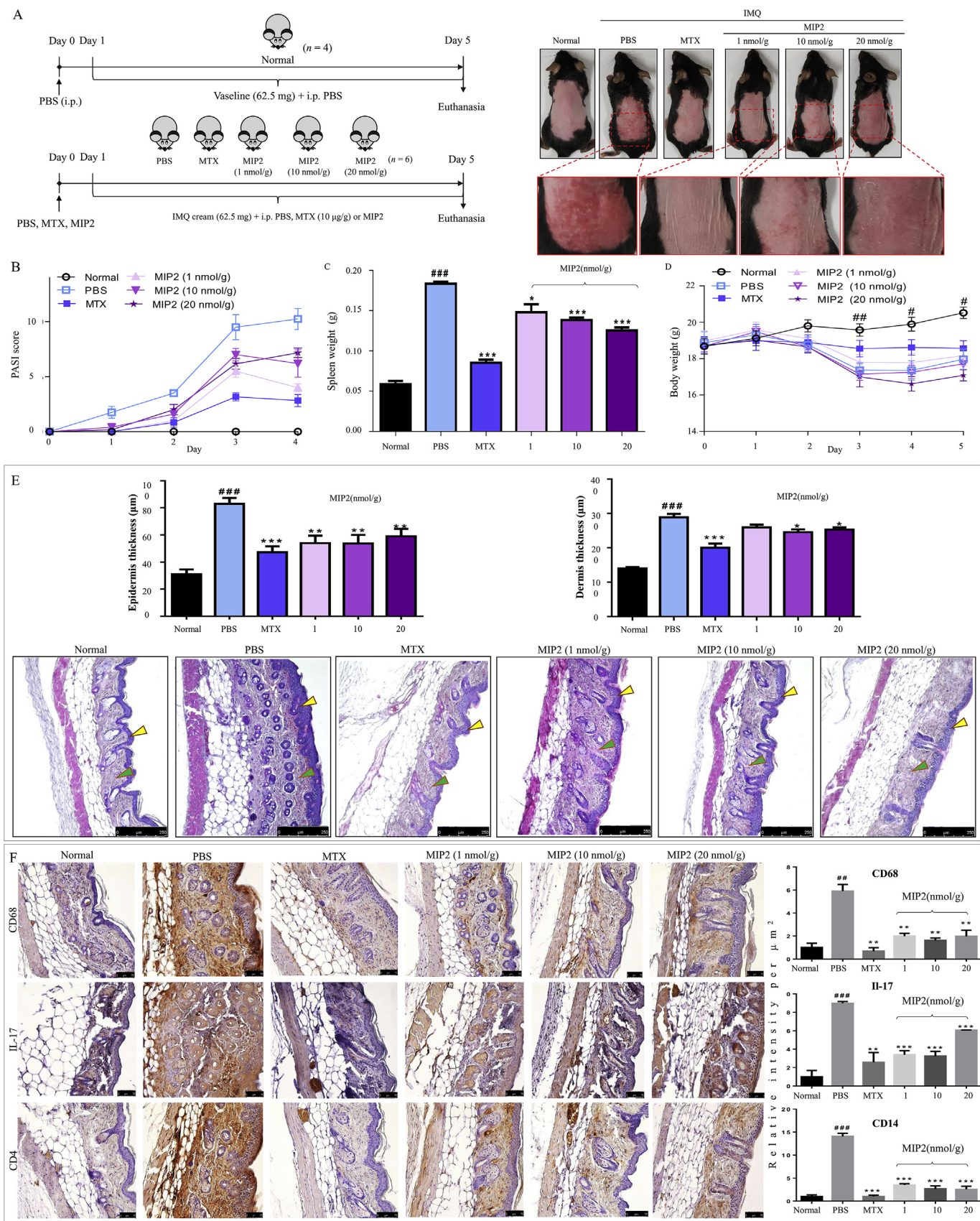


Fig. 4. Interaction of MIP2 with the TIR domain-containing proteins. (A, B) Colocalization of the FITC-MIP2 conjugate (green because of fluorescein isothiocyanate) with (A) TIRAP (red) and (B) MyD88 (yellow) in the lipopolysaccharide (LPS)-stimulated NIH3T3 cells. The scale bar represents 20 μ m. (C) A sensorgram illustrating the interaction of MIP2 with the TIR domains of MyD88, TIRAP, and TLR4. (For interpretation of the references to color in this figure legend, the reader is referred to the Web version of this article.)



(caption on next page)

Fig. 5. MIP2 ameliorates an imiquimod (IMQ)-induced psoriasis in mice. (A) The psoriasis was induced in C57BL/6 male mice by the topical application of IMQ. Three concentrations of MIP2 were i.p. administered before the IMQ application. Methotrexate (MTX) was chosen as a positive control for the relative therapeutic evaluation of MIP2. The photographs of the back skin were taken on day 4 of treatment and indicated a therapeutic benefit of MIP2 relative to the normal, untreated, and the MTX-treated groups. PBS: phosphate-buffered saline. (B) Scoring of disease severity was based on a clinical tool called the Psoriasis Area and Severity Index (PASI). The three purple lines indicate the PASI score of mice treated with MIP2 at 1 nmol/g, 10 nmol/g, and 20 nmol/g (C, D) The influence of MIP2 on the spleen weight and the body weight dynamics of the mice during the treatment regimen. (E) The impact of MIP2 on the thickness of the epidermis (yellow arrowheads) and dermis (green arrowheads). The thickness of skin in each group was measured with the Leica DMi8 fluorescence microscope (scale bar: 250 μ m). (F) Immunohistochemical analysis of lesions of the back skin in each group. The intensity of brown staining indicates CD68 expression (macrophage marker) and CD4 and IL-17 expression (Th17 cell markers) in these lesions. The scale bar is 75 μ m for high-magnification images. Data represent mean \pm SEM from five skin tissue samples of each group. *** P < 0.001 for the difference between NC and PBS, ** P < 0.01 and * P < 0.05 for the difference between groups “PBS” and “MIP2 at 1 nmol, 10 nmol, or 20 nmol” or in the MTX group, according to the two-tailed Student’s *t*-test. (For interpretation of the references to color in this figure legend, the reader is referred to the Web version of this article.)

outlined in Fig. 6A). A substantial reduction in alopecia was observed in the SLE-prone MIP2-treated mice; this symptom remained aggravated in the untreated mice (Fig. 6A). A close relation between the weight gain and up-regulation of the SLE markers (ANA, ROS, and splenomegaly) as well as damage to the heart, the kidneys, the liver, and the spleen has been reported [35]. We observed that MIP2 prevented the mice, that were fed with the standard diet, from weight gain or loss throughout the treatment period (Fig. 6B). Lymphadenopathy and splenomegaly are frequently observed symptoms in SLE patients. Approximately 50% and 10%–40% of the SLE patients develop lymphadenopathy and splenomegaly, respectively [36]. We found that the weight of lymph nodes was substantially lower in the MIP2-treated SLE-prone mice (Fig. 6C and Supplementary Fig. 2A). In case of the spleen, four out of six MIP2-treated mice exhibited a decrease in weight and an overall significant reduction in the spleen size (Fig. 6D and E, and Supplementary Fig. 2B). The levels of the characteristic SLE-associated serological markers [such as interleukins (ILs), anti-double-stranded DNA (dsDNA) antibodies, and ANA] and the urine albumin levels (associated with glomerulonephritis) increase in SLE patients and animal models [37]. Moreover, relatively low serum levels of complement components, in particular C3 and C4, are the common markers of SLE [38]. We comparatively monitored these markers in the MIP2-treated and the untreated MRL/lpr mice. Of note, we noticed that the albumin level significantly diminished in the MIP2-treated MRL/lpr mice (Fig. 6F). A substantial reduction in ANA and anti-dsDNA antibody levels was also observed as compared to untreated mice (Fig. 6G, H). A conspicuous reduction in the serum IL6 concentration was recorded; nonetheless, C3 recovery was not substantial. However, we detected an overall increased level of the serum C3 in the MIP2-treated mice (Fig. 6I and J). Next, the anti-SLE effect of MIP2 was investigated by the histological examination of mouse kidneys by H&E and PAS staining (Fig. 6K, scale bar: 100 μ m). The glomerular tuft with proliferative mesangial cells and a diffused crescent (Fig. 6K, black-dashed circles) were noticed in the untreated mice. The fibrocellular crescent was reformed and severe mesangial-cell and endothelial-cell proliferation and inflammatory-cell infiltration were substantially reversed around the glomeruli by the MIP2 treatment. Overall, these data suggested that MIP2 had a substantial curative potential against SLE.

3.7. The preventive and therapeutic effects of MIP2 on the mouse model of NASH

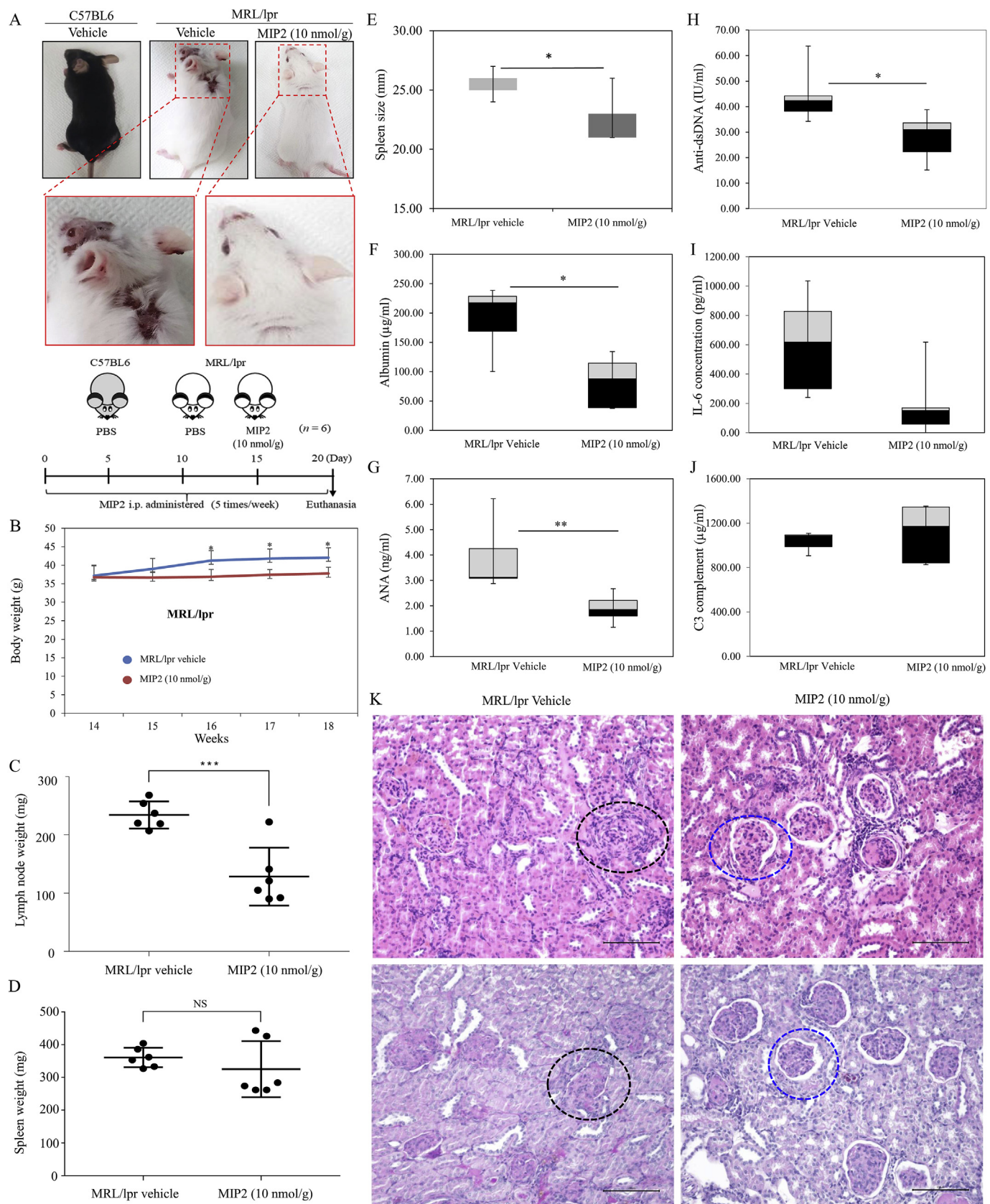
TLR4-knockout mice have been reported to be protected from the development of saturated-fat-induced insulin resistance and diet-induced obesity [39]. Other TLRs including TLR2 and TLR9 have also been reported to be associated with NASH development [40–42]. To determine whether MIP2 prevented or treated NASH, we induced NASH in 10-week-old C57BL/6J mice using the MCD diet for 6 weeks. MIP2 was i.p. injected for 6 weeks or 4 weeks as a preventive or therapeutic strategy at a dose of 10 nmol/g of the mouse weight. Liver sections subjected to H&E, the Masson’s trichrome, and the Oil red O staining revealed a severe macrovesicular fat change with moderate inflammation in the MCD diet group. Neither the MIP2-based prevention group

nor the MIP2 treatment group manifested a significant histopathological improvement of steatosis (Fig. 7A). Although there was no considerable gross change, hepatic cholesterol and triglyceride levels significantly diminished after an MIP2 administration (Fig. 7B). Serum alanine aminotransferase (AST) and aspartate aminotransferase (ALT) activity did not change significantly during the MIP2-based prevention or MIP2 treatment (Fig. 7C). Nevertheless, the hepatic expression of inflammation-related transcripts *Tnfa*, *Mcp1*, *Il-1 β* , and *Il-6* decreased with the MIP2 administration (Fig. 7D). In agreement with the MIP2-driven improvements in liver inflammation, there was a reduction in the hepatic expression of the fibrosis-related transcripts *Col*, *Fn1*, and *Acta2* (Fig. 7E). The methionine-and-choline deficiency (MCD diet) down-regulated the peroxisome proliferator-activated receptor (*Ppar*) α transcript and up-regulated the *Ppar* γ transcript, whereas MIP2 recovered the levels of both transcripts in the mouse model of the MCD diet-induced NASH (Fig. 7F).

3.8. MIP2 exerts therapeutic effects in the mouse model of LPS-induced sepsis

The up-regulation of TLR4 has been widely associated with the pathogenesis of sepsis and therefore is regarded as a potential therapeutic target [17,43–45]. Considering that TLR4 is an effective MIP2 target, we tested its anti-inflammatory potential in the model of an LPS-induced sepsis. For survival efficiency measurements, 8-week-old BALB/c mice were i.p. injected with MIP2 (10 nmol/g) 1 h before LPS injection at one of two doses: 5 μ g/g of mouse weight for a mild sepsis and 10 μ g/g of mouse weight for a severe sepsis. All the groups were thoroughly monitored for 3 days to assess their survival rates. The mice treated with 5 μ g/g LPS only, showed a 100% decrease in the survival rate within 36 h; however, co-treatment with MIP2 restored the survival rate to 20%–30% and maintained it for 3 days. Likewise, all mice injected with 10 μ g/g LPS died within 36 h; in contrast, the MIP2-treated group retained 25% survival rate for 3 days (Fig. 8A). Kidney function biomarkers such as BUN and Cr were monitored in the serum samples of normal, septic, and the MIP2-treated mice; these indicators were notably lower in the samples from the MIP2-treated mice (Fig. 8B). Furthermore, the TUNEL assay was performed to evaluate the impact of MIP2 on DNA fragmentation resulting from apoptotic signaling cascades. MIP2 remarkably decreased the number of the TUNEL-positive apoptotic cells as compared to that observed in the septic samples (Fig. 8B).

To further evaluate the anti-inflammatory effect of MIP2 on the murine sepsis model, cytokine (IL-1 β , IL-6, and TNF- α) and VEGF levels in plasma samples were assessed by ELISA. As expected, MIP2 significantly attenuated the secretion of these factors at 2 h and 24 h post-injection relative to the mice injected only with LPS (Fig. 8C and D). This phenomenon was more prominent at 24 h post-injection than at 2 h post-injection, suggesting that the peptide internalization time is a crucial factor in the peptide-based therapeutics and needs to be further improved. Overall, our findings suggest that MIP2 exerts a possible protective action against sepsis by significantly improving the survival rate of mice, reducing the systemic inflammatory response, and



(caption on next page)

Fig. 6. The therapeutic action of MIP2 on the mouse model of SLE. (A) A summary of the experimental validation of the inhibitory impact of MIP2 on SLE signs in the mouse model. A substantial reduction in alopecia was observed in the SLE-prone MIP2-treated mice. (B) The body weight remained unchanged in MIP2-treated mice throughout the treatment regimen. (C–E) Lymphadenopathy and splenomegaly significantly abated in the MIP2-treated SLE-prone mice. (F) Albumin content of urine and (G–J) serum ANA, anti-double-stranded DNA (anti-dsDNA) antibodies, IL-6, and C3 complement component were evaluated by ELISA. (K) Histological examination of the kidneys by H&E and PAS staining (scale bar: 100 μ m). A glomerular tuft with proliferative mesangial cells and a diffused crescent (black circles) were noticed in the untreated mice. The fibrocellular crescent re-formed (blue circles), and the glomeruli regained a normal shape in the MIP2-treated mice. (For interpretation of the references to color in this figure legend, the reader is referred to the Web version of this article.)

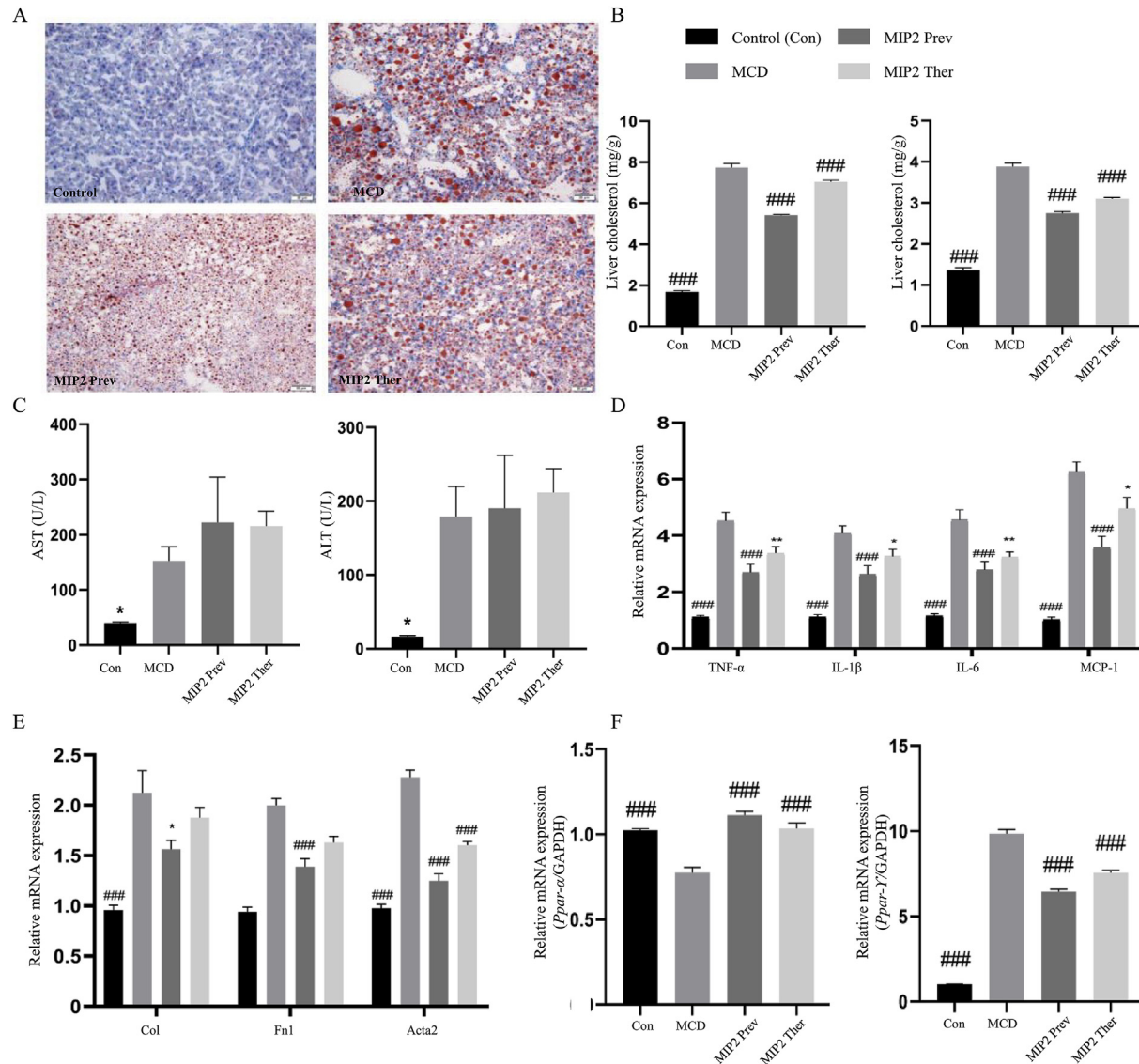


Fig. 7. The therapeutic influence of MIP2 on the mouse model of NASH. (A) Histological examination of the liver through H&E and Oil red O staining (scale bar: 50 μ m). A severe macrovesicular fat change was induced by the methionine-and-choline-deficient (MCD) diet. MIP2 did not cause a significant gross alleviation of steatosis in preventive and therapeutic groups (MIP2 Prev and MIP2 Ther, respectively). (B) Liver cholesterol and triglyceride levels of the four mouse groups. The MCD diet-induced fat change of the liver was found to be attenuated in both groups, MIP2 Prev and MIP2 Ther. Serum AST and ALT activities were not significantly reduced (were not improved) by MIP2 (C). By contrast, levels of inflammation-related (D) and fibrosis-related (E) gene transcripts were significantly diminished (improved) by MIP2 administration. (F) Dysregulated peroxisome proliferator-activated receptor ($Ppar-\alpha$) and $Ppar-\gamma$ transcript levels were restored by MIP2 administration. (For interpretation of the references to color in this figure legend, the reader is referred to the Web version of this article.)

alleviating the kidney failure in mice.

4. Discussion

Even though enormous efforts have been made to target the protein–protein interfaces (PPIs) with small-molecule inhibitors, selecting effective candidates targeting biologically crucial PPIs remains an uphill task [46]. Much work has been done to develop TLR inhibitors targeting the ligand-binding domains of TLRs [36,47]; however, the

cytoplasmic ends and their associated molecules have not been meticulously targeted. The unavailability of small-molecule inhibitors acting on the TIR domains could be partly due to the lack of a sufficient structural information, flat PPIs, and poorly-defined pockets. Targeting of the TIR domain-containing proteins may be advantageous because of their involvement in the TLR and the IL receptor signaling pathways at a high stoichiometric concentration. Nonetheless, transient protein interactions are challenging therapeutic targets. Antibody- and peptide-based therapeutics have significantly resolved the issue of undruggable

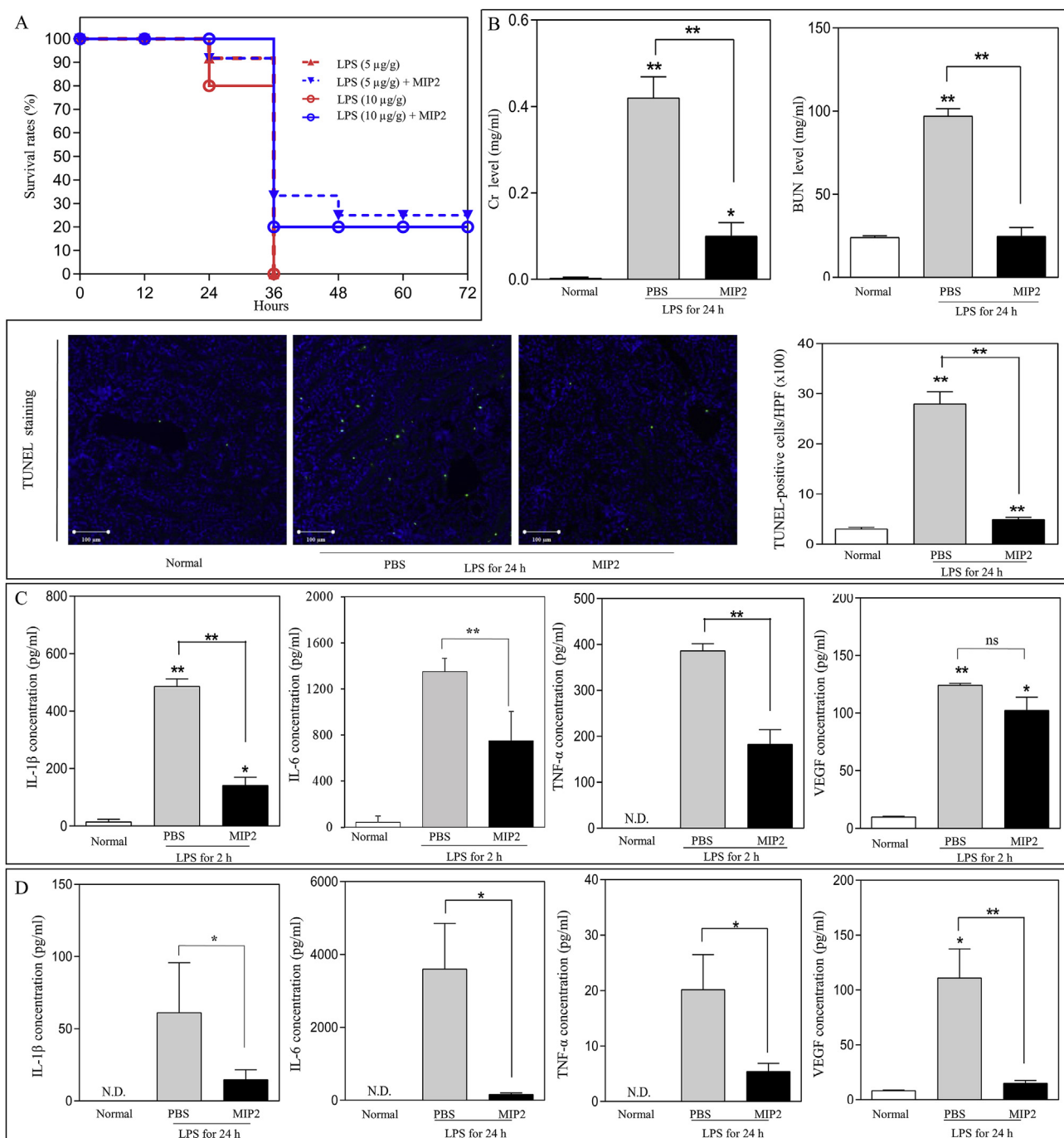


Fig. 8. The therapeutic effects of MIP2 in the mouse model of lipopolysaccharide (LPS)-induced sepsis. (A) BALB/c mice were i.p. injected with either phosphate-buffered saline (PBS) or MIP2 (10 nmol/g) for 1 h before the i.p. injection of LPS (5 µg/g or 10 µg/g), and survival rates of the mice were monitored for 3 days. (B) Levels of blood urea nitrogen (BUN) and creatinine (Cr) were measured in plasma samples. Representative photographs of the apoptotic cells in kidney tissues after terminal deoxynucleotidyl transferase dUTP nick end labeling (TUNEL) staining (scale bars represent 100 µm). The TUNEL-positive cells were quantified, and the scores have been presented in the histogram. Quantitation of IL-1 β , IL-6, TNF- α , and VEGF in plasma samples at 2 h (C) and 24 h (D) after the injection of LPS (5 µg/g). (L).

PPIs and are promising treatments. Even though peptide-based therapeutics are susceptible to enzymatic cleavage and have low bioavailability (which could be overcome by some tested techniques) [48–50], they offer lower toxicity and an enhanced target selectivity as compared to those offered by the small-molecule inhibitors. The development of a peptide or peptide mimetic is the key method for expanding the “druggable genome” by specific targeting of crucial undruggable PPIs [51].

Among the TIR domain-containing adaptors, MAL has the capacity

for bridging MyD88 with TLR [9]. Mutational studies have confirmed that the α C helix in MAL is crucial not only for MAL-MAL but also for MAL-MyD88 and MAL-TLR4 interactions [8–11]. The interstrand interface in the MAL protofilament is likely to be similar to that of MAL-MyD88 and MAL-TLR4/2 TIR-TIR interfaces [8]. The α D helix of TLR4 is likely to establish major contacts with the α C helix of MAL in this model (Fig. 1A). This suggestion was also voiced in a study by Toshchakov et al., where a peptide derived from the α D helix of TLR4 blocked the adapter recruitment to TLR4 [52]. Sharing ~40% sequence

identity and showing a structural analogy between TLR4 and TLR2, a peptide (2R9) derived from the α D helix of TLR2 blocked the recruitment of MAL to TLR2. Thus, we hypothesized that a peptide composed of the entire α C helix (comprising aa P155-to-T166) will retain its helical structure and will be sufficient to prevent the MAL TIR assembly as well as other MyD88-dependent TLR signaling, independently of entire TIR domains.

Consequently, a peptide comprising the α C helix of MAL was conjugated with one of two known CPPs (PFV and penetratin) and was tested for its interference with the ligand-induced TLR signaling. The initial SEAP assay suggested that penetratin is an efficient carrier of the peptide whereas the PFV-conjugated peptide did not exert any considerable effect (Fig. 1C). We hypothesized that this result could be due to the poor cell membrane-penetrating ability of the PFV-conjugated MIP or to some additional TLR-inhibitory property of penetratin. One report (a study unrelated to TLRs) and our further investigation suggested that neither CPP had any TLR-inhibitory action if used alone (Supplementary Fig. 1C and ref. [16]). Besides, in our ongoing study (unpublished data), we found that a computationally designed PFV-conjugated peptide effectively targeted an extracellular protein and blocked the TLR4 signaling. In addition, the PFV-conjugated peptides are internalized less effectively in a temperature-dependent manner [14,53]. A lactam bridge and disulfide bond have been widely used to restrict the conformational freedom and enhance the receptor selectivity and the binding affinity of therapeutic peptides [54–56]. Consequently, we applied a disulfide structural constraint to MIP2 (resulting in MIP3); however, MIP3 had an unexpected cytotoxic effect, whereas MIP2 did not manifest any cytotoxicity at the same concentrations (Supplementary Fig. 1A). To verify whether the c-terminal residues, especially L165, are crucial for the TLR-inhibitory effect of MIP2, its derivatives were generated by residue substitution. Of note, MIP2-1 (containing L165H and other substitutions) and MIP2-3 were found to completely lack the ability to inhibit the LPS-stimulated TLR4 signaling (Supplementary Fig. 1D, E), confirming that the c-terminal residues were crucial for this peptide's effectiveness.

The TLR-inhibitory ability of MIP2 was next evaluated in human and mouse macrophages. It is noteworthy that MIP2 not only exerted a broad-range TLR-inhibitory action but also blocked the MyD88- and the TRIF-dependent pathways of TLR4 in the LPS-stimulated RAW 264.7 cells and in the THP1-derived macrophages (Figs. 2 and 3). This finding can be partly explained by the fact that MIP2 is composed of the MAL α C helix that can bind to MAL, TLR4 TIR, and MyD88 TIR (as discussed above; Fig. 1A). Besides, MAL and TRAM are competitors, i.e., they bind to the overlapping interfaces of TLR4 TIR, and this region is likely engaged by MIP2 in both cases. A peptide that partly overlaps with the c-terminus of MIP2 has been suggested to prevent the physical interaction of MyD88 and TRAM with TLR4 and can interact with MyD88 [19,57]. Altogether, these observations reinforce the idea that MIP2 possesses a broad-range TIR domain-binding ability and hence a possible broad-range TLR-inhibitory ability. The induction of NLRP3 and a subsequent release of mature IL-1 β have been associated with TLR stimulation in a number of studies [23–25]. Both MyD88- and the TRIF-dependent TLR pathways can prime and activate the NLRP3 inflammasome [27]. We demonstrated that MIP2 inhibited the expression of NLRP3 and pro-IL-1 β in ATP-activated THP-1 cells that were primed with LPS (Fig. 3C).

The ligand-induced dimerization of the ectodomains of a TLR leads to the rearrangement of transmembrane and juxtamembrane regions, which facilitate the homotypic and heterotypic association of their TIR domains. Subsequently, this event leads to the recruitment of TIR-containing adapter molecules through a cooperative interface sharing [58–60]. The complexity and ambiguous stoichiometry of the TIR-TIR interaction has been hypothesized to be the reason for the lack of a commonly agreed interface. Overall, it is a widely accepted fact that the TIR-TIR interaction is an early event indispensable for TLR signaling. Disintegration of the TIR assembly (owing to its essential function in

TLR signaling) holds promise for ablating the TLR signaling in related immune complications. Inspired by the pivotal participation of TIRAP in TLR signaling and recent advances in peptide-based therapeutics, MIP2 was designed to negatively regulate TLR signaling by engaging the interactions of TIR domains. Our confocal imaging indicated that MIP2 colocalized with TIRAP and MyD88 and physically interacted with the TIR domains of TLR and adaptor proteins TIRAP and MyD88 (Fig. 4). The equilibrium dissociation constant (K_D) values of MIP2 with respective TIR domains of MyD88, TLR4, and TIRAP have been provided in Fig. 4C. These results suggest that the inhibitory effect of MIP2 on multiple TLR signaling pathways is likely due to its possible binding to the TIR domain-containing proteins.

The relation between TLR-signaling pathways and various human diseases, including but not limited to SLE, rheumatoid arthritis, psoriasis, sepsis, and NASH, has been shown by an expanding body of evidence [40–42,61,62]. The therapeutic properties of MIP2 were evaluated here in animal models of psoriasis, SLE, NASH, and sepsis (via peritonitis). Overall, MIP2 substantially ameliorated the IMQ-induced psoriasis symptoms and down-regulated the related biomarkers (CD68, CD4, and IL-17) in C57BL/6 mice (Fig. 5). MIP2 reduced the hallmarks of SLE (its serological markers) such as IL6, anti-dsDNA, ANA, and urine albumin and relieved SLE-associated lymphadenopathy and splenomegaly (Fig. 6). Various studies have widely implicated TLR induction in nonalcoholic fatty liver diseases. TLR4- or TLR7-knockout mice have been reported to be protected from such a liver disease [41,63]. In the present study, MIP2 decreased hepatic fat content, expression of the PPAR pathway in the mouse model of NASH induced by the MCD diet. The impact of MIP2 on NASH was more profound in the preventive strategy as compared to that in the therapeutic one (Fig. 7). The anti-inflammatory property of MIP2 was further confirmed in the model of LPS-induced sepsis. MIP2 remarkably relieved the systemic inflammatory response observed during a mild and severe form of the disease and significantly alleviated the renal damage by reducing BUN and Cr levels in blood plasma (Fig. 8).

Collectively, these *in vitro* and *in vivo* findings mean that as an inhibitor, MIP2 has broad specificity for TLRs and should be effective in alleviating autoimmune complications caused by microbial or environmental factors. Nonetheless, biological stability and potency of MIP2 may need some improvement.

Funding

This work was supported by the National Research Foundation [grant numbers NRF-2019M3A9A8065098, 2019M3D1A1078940, 2019R1A6A1A11051471] and the Ministry of Health & Welfare [grant number HI16C0992], Korea. The sponsors had no role in study design; in the collection, analysis, and interpretation of data; in the writing of the report; and in the decision to submit the article for publication.

Data availability

The raw data required to reproduce these findings are available on request.

CRediT authorship contribution statement

Masaad Shah: Conceptualization, Methodology, Formal analysis, Resources, Writing - original draft, Writing - review & editing. **Gi-Young Kim:** Investigation, Formal analysis, Writing - review & editing. **Asma Achek:** Investigation, Formal analysis, Writing - original draft, Writing - review & editing. **Eun-Young Cho:** Investigation, Formal analysis, Writing - review & editing. **Wook-Young Baek:** Investigation, Writing - review & editing. **Yang Seon Choi:** Investigation, Writing - review & editing. **Wang Hee Lee:** Investigation, Writing - review & editing. **Dong-Jin Kim:** Investigation, Writing - review & editing. **Sang**

Ho Lee: Investigation, Writing - review & editing. **Wook Kim:** Investigation, Writing - review & editing. **Soon Sun Kim:** Investigation, Writing - review & editing. **Jae Youn Cheong:** Investigation, Writing - review & editing. **Chang-Hee Suh:** Investigation, Writing - review & editing. **Sangdun Choi:** Conceptualization, Methodology, Supervision, Funding acquisition, Writing - review & editing.

Declaration of competing interest

The authors declare that they have no known competing financial interests or personal relationships that could have appeared to influence the work reported in this paper.

Appendix A. Supplementary data

Supplementary data to this article can be found online at <https://doi.org/10.1016/j.biomaterials.2020.119974>.

References

- [1] S. Akira, S. Uematsu, O. Takeuchi, Pathogen recognition and innate immunity, *Cell* 124 (4) (2006) 783–801.
- [2] T. Ve, N.J. Gay, A. Mansell, B. Kobe, S. Kellie, Adaptors in toll-like receptor signalling and their potential as therapeutic targets, *Curr. Drug Targets* 13 (11) (2012) 1360–1374.
- [3] N.J. Gay, M.F. Symmons, M. Gangloff, C.E. Bryant, Assembly and localization of Toll-like receptor signalling complexes, *Nat. Rev. Immunol.* 14 (8) (2014) 546–558.
- [4] L. Vyncke, C. Bovijn, E. Pauwels, T. Van Acker, E. Ryssinck, E. Burg, J. Tavernier, F. Peelman, Reconstructing the TIR side of the myddosome: a paradigm for TIR-TIR interactions, *Structure* 24 (3) (2016) 437–447.
- [5] C. Bovijn, P. Ulrichs, A.S. De Smet, D. Catteeuw, R. Beyaert, J. Tavernier, F. Peelman, Identification of interaction sites for dimerization and adapter recruitment in Toll/interleukin-1 receptor (TIR) domain of Toll-like receptor 4, *J. Biol. Chem.* 287 (6) (2012) 4088–4098.
- [6] C.J. Chen, H. Kono, D. Golenbock, G. Reed, S. Akira, K.L. Rock, Identification of a key pathway required for the sterile inflammatory response triggered by dying cells, *Nat. Med.* 13 (7) (2007) 851–856.
- [7] E. Guven-Maiorov, O. Keskin, A. Gursoy, C. VanWaes, Z. Chen, C.J. Tsai, R. Nussinov, The architecture of the TIR domain signalosome in the toll-like receptor-4 signaling pathway, *Sci. Rep.* 5 (2015) 13128.
- [8] T. Ve, P.R. Vajjhala, A. Hedger, T. Croll, F. DiMaio, et al., Structural basis of TIR-domain-assembly formation in MAL- and MyD88-dependent TLR4 signaling, *Nat. Struct. Mol. Biol.* 24 (9) (2017) 743–751.
- [9] Z. Lin, J. Lu, W. Zhou, Y. Shen, Structural insights into TIR domain specificity of the bridging adaptor Mal in TLR4 signaling, *PLoS One* 7 (4) (2012) e34202.
- [10] C. Bovijn, A.S. Desmet, I. Uyttendaele, T. Van Acker, J. Tavernier, F. Peelman, Identification of binding sites for myeloid differentiation primary response gene 88 (MyD88) and Toll-like receptor 4 in MyD88 adapter-like (Mal), *J. Biol. Chem.* 288 (17) (2013) 12054–12066.
- [11] E. Valkov, A. Stamp, F. Dimaio, D. Baker, B. Verstak, et al., Crystal structure of Toll-like receptor adaptor MAL/TIRAP reveals the molecular basis for signal transduction and disease protection, *Proc. Natl. Acad. Sci. U. S. A.* 108 (36) (2011) 14879–14884.
- [12] L.A. Couture, W. Piao, L.W. Ru, S.N. Vogel, V.Y. Toshchakov, Targeting Toll-like receptor (TLR) signaling by Toll/interleukin-1 receptor (TIR) domain-containing adapter protein/MyD88 adapter-like (TIRAP/Mal)-derived decoy peptides, *J. Biol. Chem.* 287 (29) (2012) 24641–24648.
- [13] S. Park, H.J. Shin, M. Shah, H.Y. Cho, M.A. Anwar, et al., TLR4/MD2 specific peptides stalled in vivo LPS-induced immune exacerbation, *Biomaterials* 126 (2017) 49–60.
- [14] M. Rhee, P. Davis, Mechanism of uptake of C105Y, a novel cell-penetrating peptide, *J. Biol. Chem.* 281 (2) (2006) 1233–1240.
- [15] D. Derossi, A.H. Joliot, G. Chassaing, A. Prochiantz, The third helix of the Antennapedia homeodomain translocates through biological membranes, *J. Biol. Chem.* 269 (14) (1994) 10444–10450.
- [16] C.B. de Araujo, L.C. Russo, L.M. Castro, F.L. Forti, E.R. do Monte, V. Rioli, F.C. Gozzo, A. Colquhoun, E.S. Ferro, A novel intracellular peptide derived from g1/s cyclin d2 induces cell death, *J. Biol. Chem.* 289 (24) (2014) 16711–16726.
- [17] H.K. Kwon, M.C. Patra, H.J. Shin, X. Gui, A. Achek, et al., A cell-penetrating peptide blocks Toll-like receptor-mediated downstream signaling and ameliorates autoimmune and inflammatory diseases in mice, *Exp. Mol. Med.* 51 (4) (2019) 50.
- [18] M. Yamamoto, S. Sato, H. Hemmi, S. Uematsu, K. Hoshino, T. Kaihara, O. Takeuchi, K. Takeda, S. Akira, TRAM is specifically involved in the Toll-like receptor 4-mediated MyD88-independent signaling pathway, *Nat. Immunol.* 4 (11) (2003) 1144–1150.
- [19] W. Piao, S.N. Vogel, V.Y. Toshchakov, Inhibition of TLR4 signaling by TRAM-derived decoy peptides in vitro and in vivo, *J. Immunol.* 190 (5) (2013) 2263–2272.
- [20] K. Honda, T. Taniguchi, IRFs: master regulators of signalling by Toll-like receptors and cytosolic pattern-recognition receptors, *Nat. Rev. Immunol.* 6 (9) (2006) 644–658.
- [21] J.Y. Kim, S.J. Park, K.J. Yun, Y.W. Cho, H.J. Park, K.T. Lee, Isoliquiritigenin isolated from the roots of Glycyrrhiza uralensis inhibits LPS-induced iNOS and COX-2 expression via the attenuation of NF-kappaB in RAW 264.7 macrophages, *Eur. J. Pharmacol.* 584 (1) (2008) 175–184.
- [22] A.P. West, I.E. Brodsky, C. Rahner, D.K. Woo, H. Erdjument-Bromage, et al., TLR signalling augments macrophage bactericidal activity through mitochondrial ROS, *Nature* 472 (7344) (2011) 476–480.
- [23] F.G. Bauerfeind, G. Horvath, A. Stutz, E.S. Alnemri, K. MacDonald, et al., Cutting edge: NF-kappaB activating pattern recognition and cytokine receptors license NLRP3 inflammasome activation by regulating NLRP3 expression, *J. Immunol.* 183 (2) (2009) 787–791.
- [24] L. Franchi, T. Eigenbrod, G. Nunez, Cutting edge: TNF-alpha mediates sensitization to ATP and silica via the NLRP3 inflammasome in the absence of microbial stimulation, *J. Immunol.* 183 (2) (2009) 792–796.
- [25] Y. Xing, X. Yao, H. Li, G. Xue, Q. Guo, G. Yang, L. An, Y. Zhang, G. Meng, Cutting edge: TRAF6 mediates TLR/IL-1R signaling-induced nontranscriptional priming of the NLRP3 inflammasome, *J. Immunol.* 199 (5) (2017) 1561–1566.
- [26] S.P. Cullen, C.J. Kearney, D.M. Clancy, S.J. Martin, Diverse activators of the NLRP3 inflammasome promote IL-1beta secretion by triggering necrosis, *Cell Rep.* 11 (10) (2015) 1535–1548.
- [27] T. Fernandes-Alnemri, S. Kang, C. Anderson, J. Sagara, K.A. Fitzgerald, E.S. Alnemri, Cutting edge: TLR signaling licenses IRAK1 for rapid activation of the NLRP3 inflammasome, *J. Immunol.* 191 (8) (2013) 3995–3999.
- [28] K.A. Fitzgerald, D.C. Rowe, B.J. Barnes, D.R. Caffrey, A. Visintin, E. Latz, B. Monks, P.M. Pitha, D.T. Golenbock, LPS-TLR4 signaling to IRF-3/7 and NF-kappaB involves the toll adaptors TRAM and TRIF, *J. Exp. Med.* 198 (7) (2003) 1043–1055.
- [29] M.P. Schon, W.H. Boehncke, E.B. Brocker, Psoriasis: clinical manifestations, pathogenesis and therapeutic perspectives, *Discov. Med.* 5 (27) (2005) 253–258.
- [30] B.S. Baker, J.M. Ovigne, A.V. Powles, S. Corcoran, L. Fry, Normal keratinocytes express Toll-like receptors (TLRs) 1, 2 and 5: modulation of TLR expression in chronic plaque psoriasis, *Br. J. Dermatol.* 148 (4) (2003) 670–679.
- [31] T. Hirai, T. Kanda, K. Sato, M. Takaishi, K. Nakajima, M. Yamamoto, R. Kamijima, J. Diiovanni, S. Sano, Cathepsin K is involved in development of psoriasis-like skin lesions through TLR-dependent Th17 activation, *J. Immunol.* 190 (9) (2013) 4805–4811.
- [32] E. Carceller, M. Ballegeer, J. Deckers, C. Riccardi, S. Bruscoli, T. Hochepied, C. Libert, P. Perez, Overexpression of Glucocorticoid-induced Leucine Zipper (GILZ) increases susceptibility to Imiquimod-induced psoriasis and involves cutaneous activation of TGF-beta1, *Sci. Rep.* 6 (2016) 38825.
- [33] S.P. Jin, S.J. Koh, D.A. Yu, M.W. Kim, H.T. Yun, D.H. Lee, H.S. Yoon, S. Cho, H.S. Park, Imiquimod-applied Interleukin-10 deficient mice better reflects severe and persistent psoriasis with systemic inflammatory state, *Exp. Dermatol.* 27 (1) (2018) 43–49.
- [34] Y.W. Wu, W. Tang, J.P. Zuo, Toll-like receptors: potential targets for lupus treatment, *Acta Pharmacol. Sin.* 36 (12) (2015) 1395–1407.
- [35] J.E. Toller-Kawahisa, N.C. Canicoba, V.P. Venancio, R. Kawahisa, L.M. Antunes, T.M. Cunha, C.M. Marzocchi-Machado, Systemic lupus erythematosus onset in lupus-prone B6.MRL/lpr mice is influenced by weight gain and is preceded by an increase in neutrophil oxidative burst activity, *Free Radic. Biol. Med.* 86 (2015) 362–373.
- [36] F. Bashal, Hematological disorders in patients with systemic lupus erythematosus, *Open Rheumatol. J.* 7 (2013) 87–95.
- [37] J.J. Weening, V.D. Agati, M.M. Schwartz, S.V. Seshan, C.E. Alpers, et al., The classification of glomerulonephritis in systemic lupus erythematosus revisited, *Kidney Int.* 65 (2) (2004) 521–530.
- [38] V. Sandhu, M. Quan, SLE and serum complement: causative, concomitant or coincidental? *Open Rheumatol. J.* 12 (2018) 171.
- [39] D.M. Tsukumo, M.A. Carvalho-Filho, J.B. Carvalheira, P.O. Prada, S.M. Hirabara, et al., Loss-of-function mutation in Toll-like receptor 4 prevents diet-induced obesity and insulin resistance, *Diabetes* 56 (8) (2007) 1986–1998.
- [40] T. Csak, A. Velayudham, I. Hritz, J. Petrasek, I. Levin, et al., Deficiency in myeloid differentiation factor-2 and toll-like receptor 4 expression attenuates nonalcoholic steatohepatitis and fibrosis in mice, *Am. J. Physiol. Gastrointest. Liver Physiol.* 300 (3) (2011) G433–G441.
- [41] C.A. Rivera, P. Adegboyega, N. van Rooijen, A. Tagalicud, M. Allman, M. Wallace, Toll-like receptor-4 signaling and Kupffer cells play pivotal roles in the pathogenesis of non-alcoholic steatohepatitis, *J. Hepatol.* 47 (4) (2007) 571–579.
- [42] K. Miura, Y. Kodama, S. Inokuchi, S. Schnabl, T. Aoyama, H. Ohnishi, J.M. Olefsky, D.A. Brenner, E. Seki, Toll-like receptor 4 promotes steatohepatitis by induction of interleukin-1beta in mice, *Gastroenterology* 139 (1) (2010) 323–334.
- [43] N.N. Kuzmich, K.V. Sivak, V.N. Chubarev, Y.B. Porozov, T.N. Savateeva-Lyubimova, F. Peri, TLR4 Signaling Pathway Modulators as Potential Therapeutics in Inflammation and Sepsis, *Vaccines (Basel)* vol. 5, (4) (2017) 34.
- [44] Q. Li, C. Wu, Z. Liu, H. Zhang, Y. Du, Y. Liu, K. Song, Q. Shi, R. Li, Increased TLR4 expression aggravates sepsis by promoting IFN-gamma expression in CD38(-/-) mice, *J. Immunol. Res.* 2019 (2019) e3737890.
- [45] X. Liu, M. Wen, X. Li, L. Chen, J. Zeng, Y. Deng, H. Zeng, β 1 receptor blocker decreases the myocardial inflammation in the sepsis adult rats through inhibition of TLR4/NF-kappaB signaling pathway, *Zhonghua Wei Zhong Bing Ji Jiu Yi Xue* 31 (2) (2019) 193–197.
- [46] J.A. Wells, C.L. McLendon, Reaching for high-hanging fruit in drug discovery at protein-protein interfaces, *Nature* 450 (7172) (2007) 1001–1009.
- [47] X. Wang, C. Smith, H. Yin, Targeting Toll-like receptors with small molecule agents, *Chem. Soc. Rev.* 42 (12) (2013) 4859–4866.
- [48] A. Newland, M.T. Caulier, M. Kappers-Klunne, M.R. Schipperus, F. Lefrere,

- J.J. Zwaginga, J. Christal, C.F. Chen, J.L. Nichol, An open-label, unit dose-finding study of AMG 531, a novel thrombopoiesis-stimulating peptibody, in patients with immune thrombocytopenic purpura, *Br. J. Haematol.* 135 (4) (2006) 547–553.
- [49] A. Coxon, J. Bready, H. Min, S. Kaufman, J. Leal, et al., Context-dependent role of angiopoietin-1 inhibition in the suppression of angiogenesis and tumor growth: implications for AMG 386, an angiopoietin-1/2-neutralizing peptibody, *Mol. Canc. Therapeut.* 9 (10) (2010) 2641–2651.
- [50] H. Hsu, S.D. Khare, F. Lee, K. Miner, Y.L. Hu, et al., A novel modality of BAFF-specific inhibitor AMG623 peptibody reduces B-cell number and improves outcomes in murine models of autoimmune disease, *Clin. Exp. Rheumatol.* 30 (2) (2012) 197–201.
- [51] A.L. Hopkins, C.R. Groom, The druggable genome, *Nat. Rev. Drug Discov.* 1 (9) (2002) 727–730.
- [52] V.Y. Toshchakov, H. Szmacinski, L.A. Couture, J.R. Lakowicz, S.N. Vogel, Targeting TLR4 signaling by TLR4 Toll/IL-1 receptor domain-derived decoy peptides: identification of the TLR4 Toll/IL-1 receptor domain dimerization interface, *J. Immunol.* 186 (8) (2011) 4819–4827.
- [53] C.L. Watkins, P. Brennan, C. Fegan, K. Takayama, I. Nakase, S. Futaki, A.T. Jones, Cellular uptake, distribution and cytotoxicity of the hydrophobic cell penetrating peptide sequence PFVYLI linked to the proapoptotic domain peptide PAD, *J. Contr. Release* 140 (3) (2009) 237–244.
- [54] M. Choref, E. Roubini, R.L. McKee, S.W. Gibbons, M.E. Goldman, M.P. Caulfield, M. Rosenblatt, Cyclic parathyroid hormone related protein antagonists: lysine 13 to aspartic acid 17 [i to (i + 4)] side chain to side chain lactamization, *Biochemistry* 30 (24) (1991) 5968–5974.
- [55] R.S. Harrison, N.E. Shepherd, H.N. Hoang, G. Ruiz-Gomez, T.A. Hill, et al., Downsizing human, bacterial, and viral proteins to short water-stable alpha helices that maintain biological potency, *Proc. Natl. Acad. Sci. U. S. A.* 107 (26) (2010) 11686–11691.
- [56] A. Achek, M. Shah, J.Y. Seo, H.-K. Kwon, X. Gui, et al., Linear and rationally designed stapled peptides abrogate TLR4 pathway and relieve inflammatory symptoms in rheumatoid arthritis rat model, *J. Med. Chem.* 62 (14) (2019) 6495–6511.
- [57] W. Piao, K.A. Shirey, L.W. Ru, W. Lai, H. Szmacinski, et al., A decoy peptide that disrupts TIRAP recruitment to TLRs is protective in a murine model of influenza, *Cell Rep.* 11 (12) (2015) 1941–1952.
- [58] Y. Xu, X. Tao, B. Shen, T. Horng, R. Medzhitov, J.L. Manley, L. Tong, Structural basis for signal transduction by the Toll/interleukin-1 receptor domains, *Nature* 408 (6808) (2000) 111–115.
- [59] R. Nunez Miguel, J. Wong, J.F. Westoll, H.J. Brooks, L.A. O'Neill, N.J. Gay, C.E. Bryant, T.P. Monie, A dimer of the Toll-like receptor 4 cytoplasmic domain provides a specific scaffold for the recruitment of signalling adaptor proteins, *PLoS One* 2 (8) (2007) e788.
- [60] T.P. Monie, M.C. Moncrieffe, N.J. Gay, Structure and regulation of cytoplasmic adapter proteins involved in innate immune signaling, *Immunol. Rev.* 227 (1) (2009) 161–175.
- [61] L. Duffy, S.C. O'Reilly, Toll-like receptors in the pathogenesis of autoimmune diseases: recent and emerging translational developments, *ImmunoTargets Ther.* 5 (2016) 69.
- [62] A. Achek, D. Yesudhas, S. Choi, Toll-like receptors: promising therapeutic targets for inflammatory diseases, *Arch Pharm. Res. (Seoul)* 39 (8) (2016) 1032–1049.
- [63] Y.S. Roh, J.W. Kim, S. Park, C. Shon, S. Kim, S.K. Eo, J.K. Kwon, C.W. Lim, B. Kim, Toll-like receptor-7 signaling promotes nonalcoholic steatohepatitis by inhibiting regulatory T cells in mice, *Am. J. Pathol.* 188 (11) (2018) 2574–2588.